University of Crete

Department of Physics

Master's Thesis

Non-Hermitian jumps in disordered lattices

Author:
Andronikos Leventis

Supervisors:
Prof. K. Makris
Prof. E. N. Economou

Thesis submitted toward partial fulfillment of the requirements of the degree of MSc in Physics

Heraklion, October 2022

This page intentionally left blank.

Acknowledgments

First and foremost, I would like to thank my supervisors Prof. K. Makris and Prof. E. N. Economou for providing their experienced guidance toward the completion of this work.

Prof. E. N. Economou has been an inspiration in my last three years as a student in UOC. His luscious and comprehensive presentation of topics in various areas, especially in -but not limited to- condensed matter, has been immensely helpful in my understanding of Physics.

I would also like to thank Prof. K. Makris for providing constant motivation and guidance throughout this project, as well as introducing me to the field of optics. Our discussions have been insightful and his help was critical to this project's completion.

Furthermore, I am sincerely grateful to the UOC faculty members who have done their best, despite great difficulties during the COVID-19 pandemic, to provide a stimulating educational experience with great dedication throughout the past years.

Περίληψη

Το αντικείμενο αυτής της εργασίας είναι η μελέτη μιας νέας και απρόσμενης μορφής κυματικής διάδοσης η οποία εμφανίζεται στη δυναμική ορισμένων μη-Ερμιτιανών τυχαίων πλεγμάτων (¨αποεντοπισμός μέσω αλμάτων¨), στην οποία το προφίλ διάδοσης του κανονικοποιημένου πεδίου κατά την διάδοση μιας αρχικής διέγερσης εμφανίζει έναν αντιδιαισθητικό μηχανισμό διάδοσης μέσω κβαντισμένων ¨αλμάτων' παρά τον ισχυρό εντοπισμό των ιδιοκαταστάσεων του πλέγματος λόγω της τυχαιότητας. Η εργασία αρχικά εστιάζει σε μονοδιάστατες αλυσίδες ασθενώς συζευγμένων κυματοδηγών που εμφανίζουν απώλεια ή ενίσχυση με τυχαία κατανεμημένο τρόπο, και έπειτα στρέφεται σε διατάξεις μη-αμοιβαία συζευγμένων κυματοδηγών που περιγράφονται από το μοντέλο των Χάτανο-Νέλσον. Η προέλευση των μη-Ερμιτιανών αλμάτων που εμφανίζονται σε αυτά τα συστήματα για συγκεκριμένα είδη τυχαιότητας αποκαλύπτεται εξετάζοντας τις σχετικές φασματικές τους ιδιότητες που προκύπτουν από την μη-Ερμιτιανότητα τους, όπως η μη-ορθογωνιότητα των ιδιοκαταστάσεών τους. Τέλος, παρουσιάζονται επιπλέον η επίδραση του μη-Ερμιτιανού skin effect στον αποεντοπισμό μέσω αλμάτων καθώς και μια γενίκευση των αποτελεσμάτων για τυχαία διδιάστατα πλέγματα.

Abstract

The subject of this thesis is to study the appearance of a new and unexpected form of wave propagation that appears in the dynamics of certain non-Hermitian random lattices, namely "delocalization via jumps", wherein the normalized field profile of the evolution of an initial excitation exhibits a counterintuitive propagation mechanism via quantized jumps despite the strong disorder induced localization of the eigenstates of the lattice. The dynamics of such systems is explored and the physical mechanism behind such an effect is elucidated in the context of non-Hermitian Anderson localization. This work initially focuses in one-dimensional chains of evanescently coupled waveguides exhibiting randomly distributed gain or loss, and then shifts its focus to arrays of non-reciprocally coupled waveguides described by the Hatano-Nelson model. The origin of the non-Hermitian jumps that are exhibited by such systems for certain types of disorder is then uncovered by examining their relevant spectral properties that arise from their non-Hermiticity, such as the non-orthogonality of their eigenstates. Finally, the impact of the non-Hermitian skin effect (NHSE) on the jumpy dynamics as well as a generalization of our results for in two-dimensional tight-binding lattices are also presented.

Output: A. Leventis, K. G. Makris, and E. N. Economou, Phys. Rev. B **106**, 064205 (2022)

Contents

List of commonly used symbols

To avoid confusion relating to the indices used throughout the chapters of this work, n will be used to index the N sites of a lattice and j will be used to index the N eigenstates and eigenvalues of the Hamiltonian corresponding to the same lattice.

N	the size of a one 1D-lattice
M, N	the number of rows and columns in a 2D-lattice
ϵ_n	On-site potential on the site with index n
c	the coupling constant, usually taken to be $c = 1$, in the tight-binding Hamiltonian
W	disorder strength in the case of a diagonal disorder term drawn from a rectangular distribution; if the disorder is complex, W_R and W_I is the disorder strength for the real and imaginary part of the disorder respectively
z, z_i	propagation distance; if taken in a discretized interval with step dz, $z_i = i \cdot dz$
ψ_n	the complex field amplitude of a field $\|\psi\rangle$ on the n-th site of a lattice
$\mathcal{P}(z)$	the optical power of the field $\|\psi(z)\rangle$, defined as $\mathcal{P}(z) = \sum_{n=1}^{N} \|\psi_n(z)\|^2$
ϕ_n	the normalized field amplitude on the n-th site, defined as $\phi_n(z) = \psi_n(z)/\sqrt{\mathcal{P}(z)}$ for each component
$\|u_j\rangle$	the j-th eigenstate of the Hamiltonian referring to a lattice of size N; if the Hamiltonian is non-Hermitian, u_j^L and u_j^R refer to left and right eigenstates respectively
u_{jn}	the n-th component of the j-th eigenstate; see above
ω_j	the eigenvalue corresponding to the j-th eigenstate
γ_j	the imaginary part of ω_j
c_j	the projection coefficient of the field $\|\psi\rangle$ on the j-th eigenstate, defined as $\langle u_j^L \|\psi\rangle$ in general
V	the disorder strength of off-diagonal disorder drawn from an equal-probability distribution corresponding to a disk of radius V in the complex plane

Chapter 1

Introduction

The spectral and dynamical behavior of periodic systems, such as atoms in a crystalline structure, are determined by the application of Bloch's theorem, which states that the eigenstates of a periodic system behave as the product of a plane wave and a function of the same periodicity. As a result of this theorem, the eigenstates extend over the entirety of the system; this also explains why in metals, one can may derive properties such as resistivity or the specific heat capacity with some accuracy using a one-body approximation. In actual materials, there exist non-periodic defects (such as inclusions or dislocations) that cause deviations from periodicity. Such perturbations result in diffusive transport instead of the ballistic one associated with perfect order; the diffusive transport is associated with eigenstates extended over the whole length of the system but with a randomized phase characterized by the so-called phase coherence length. Moreover, Bloch's theorem is usually coupled with periodic boundary conditions for the ends of the system; the application of closed boundary conditions results in the appearance of edge states in the spectrum which are not described by Bloch's theorem. In practice, for a large system approaching the thermodynamic limit $N \to \infty$, the spectrum does not differ significantly when considering these states.

However, for sufficiently strong disorder, a new regime arises wherein some eigenstates become localized([1] - [4]); in the case of a crystal lattice, the spatial wavefunction describing an electron may be confined to a narrow region of the lattice. An immediate result of this effect is the absence of transport in such a system, wherein waves do not propagate outside a confined region of the lattice characterized by a localization length ξ. The cause of this effect, known as Anderson localization [1], has been determined to be the constructive interference of waves following multiple closed paths about a point inside the medium; in the presence of sufficiently strong random scatterers, this process increases the probability of finding the electron in its starting position. Localized states do not contribute to the conductivity. For an infinite 1D disordered system, where all states are localized, the conductivity is hence zero; such a situation is termed an Anderson insulator.

Disordered systems have been the focus of extensive studies in the past decades since the publication of Anderson's prolific paper regarding the localization of electrons in disordered crystals. Since then, Anderson localization has been observed not only in electronic, but also in other systems where wave propagation and disorder is involved, such as mechanical and optical systems, in the quantum and classical domains alike ([2] - [7]). In the last case in particular, experiments involving disorder in optical waveguides have provided new insights in regard to localization in two and three dimensions as well as numerous technological applications. While exact control of wave propagation in a complex medium is a difficult task, the field of photonics has provided fertile ground for investigating Anderson localization through novel experimental techniques involving waveguide arrays and fiber networks ([14]-[18]). Furthermore, photons do not interact with each other and therefore such experiments avoid the complexity associated with many-body electron interactions present in solid state lattices.

Non-Hermiticity, a property associated with open systems that exchange energy with their environment, has also recently become the focus of recent discoveries, turning one of the core postulates of quantum mechanics on its head. The initial discovery of $\mathcal{PT}$-symmetrical systems and their properties by Bender and Boettcher ([19] - [21]) and the subsequent implementation of $\mathcal{PT}$-symmetric lattices in optical systems ([22] - [27]) has given rise to the field of non-Hermitian photonics. In this field the concept of optical loss, inherent to optical systems and traditionally considered an obstacle, has been exploited in conjunction with gain to generate new physics such as exceptional points in $\mathcal{PT}$-symmetric lattices ([28]-[34]), the non-Hermitian skin effect exhibited in non-reciprocal photonic lattices ([67]-[71]), topological non-Hermitian lattices [46] and constant intensity waves in disordered media (thus exploiting wave transport) ([49] - [51]. The associated technological advances included novel metamaterials ([35]-[36]), optical isolators and switches ([34] - [44]) as well as ultra-sensitive sensors utilizing EPs [45].

A photonic lattice, consisting of an array of coupled waveguides, is equivalent to a crystal lattice consisting of periodically ordered atoms as potential wells; in the paraxial approximation, the transverse direction of the field is analogous to the wavefunction in Schrödinger's equation and the refractive index takes the role of the potential. Therefore, by controlling the refractive index on each waveguide site, one can emulate the propagation of a wave in a solid crystal ([13], [47]). The introduction of gain and loss can also be achieved by accordingly modifying the imaginary part of the refractive index; in this case, gain corresponds to on-site optical pumping and loss to cavity leaks or absorption by the material. By randomly varying the real and imaginary part of the refractive index on each site, the eigenstates of the system become localized while its spectrum varies in the complex plane; this non-Hermitian version of Anderson localization ([54] - [57]) provides new emergent effects that are still largely unexplored.

An additional possibility that appears in the context of non-Hermitian photonics is the implementation of non-reciprocal coupling resulting in non-symmetric wave propagation. Such an effect is possible by amplifying forward propagating waves, thus inducing a preferred direction of propagation in the

lattice[68]. A prototypical non-Hermitian model that has been extensively studied in this context was originally introduced by Hatano and Nelson ([61] - [63]). In the case of a disordered Hatano-Nelson lattice, the imbalance between the couplings counterbalances the effect of disorder and prevents localization for some of the eigenstates, introducing a delocalization transition [60]. Furthermore, the eigenvalues and eigenstates of such a system exhibit high sensitivity to the topology (boundary conditions) of the lattice, in sharp contrast to the Hermitian case. This effect, known as the non-Hermitian skin effect (NHSE) ([65], [67]), is a novel property of non-Hermitian systems that also occurs in other non-Hermitian models and lattices in higher dimensions that display skin modes which feature characteristically in the topology of their spectrum.

Whereas the absence of transport in Hermitian disordered lattices has been thoroughly investigated in the context of Anderson localization, the field of non-Hermitian localization remains largely unexplored and presents the intriguing possibility of wave transport even in the presence of strong disorder [59]. In particular, the additional degree of freedom provided by the non-Hermiticity of the system provides an avenue for the construction of loss-free propagation ([49]-[50]). A recent experiment [58] has demonstrated the appearance of an unexpected and counterintuitive form of wave propagation in random non-Hermitian lattices characterized by a rectangular distribution, despite the strong localization of the eigenstates. In this work, this dynamical effect ("delocalization via jumps") is studied in order to provide a systematic methodology toward the prediction of the location, number and duration of these jumps. The main focus is the non-Hermitian tight binding Anderson lattice and the asymmetrical Hatano-Nelson lattice with disorder, which both display this mode of propagation under certain conditions which are established. A brief introduction to the relevant spectral properties of these systems is made before an investigating their dynamics. The relevance of the NHSE to this form of propagation, the question of transport vs amplification as well as the dynamics of two-dimensional non-Hermitian disordered lattices are also systematically discussed.

Chapter 2

The 1-D tight-binding Anderson model

In this chapter we briefly introduce Anderson localization as it manifests in a one-dimensional disordered tight-binding lattice model, as well the computational techniques that were employed in the calculation of the localization length of its eigenstates and the dynamics of wave propagation on the lattice. We later introduce non-Hermitian localization in the corresponding non-Hermitian model and discuss its differences to the Hermitian case as well as the new propagation effects that appear in this kind of lattice.

2.1 Hermitian disordered lattices

2.1.1 Localization length

The tight-binding Hamiltonian is derived by considering only nearest neighbor interactions in a lattice where the cites are periodically situated. Such a lattice is described by the on-site self-energy ϵ_n, which for a lattice with only one kind of lattice site is taken to be constant $\epsilon_n = \epsilon \, \forall n$, as well as a coupling constant $c_{n,m}$ between neighboring sites which here we also take to be constant and real ($c_{n,n'} = c$) [12]. In the case of a system of size N, this Hamiltonian then takes the form of a matrix with only diagonal and off-diagonal elements:

$$\hat{H} = \sum_{n=1}^{N} \epsilon_n \left|n\right\rangle \left\langle n\right| + \sum_{n,n'}{}' c \left|n\right\rangle \left\langle n'\right| \tag{2.1}$$

where the accented sum denotes summation over nearest neighbors ($|n - n'| = 1$), and c is a real coupling constant between the two sites.

The dynamics of this system is described by the complex field in vectorized form $|\psi\rangle = (\psi_1, \psi_2, \ldots, \psi_N)$ where ψ_n is the field amplitude on the n-th site of the lattice. Taking $\epsilon_n = \epsilon \forall n$, an eigenfunction $|\psi\rangle_j$ of this Hamiltonian then

solves the system of N linear equations:

$$\omega\psi_{j,n} = \epsilon\psi_{j,n} + c(\psi_{j,n+1} + \psi_{j,n-1}) \tag{2.2}$$

where ω_j denotes its respective eigenvalue. In the case of periodic boundary conditions (PBC), we can apply Bloch's theorem by demanding that $\psi_{j,n} = N^{-1/2}e^{ik_j n}$ are the solutions in terms of the wavevector k. In this case, the eigenvalues of the Hamiltonian in Eq. (2.2) turn out to be given by the dispersion relation $\omega(k_j) = \epsilon + 2c\cos(k_j)$. For an infinite system, this is a continuous band with $-\pi < k < \pi$. We may take $\epsilon = 0$ as a non-zero ϵ results simply in a global eigenvalue shift. Furthermore, we take by convention $c = 1$ for the rest of this section.

The above Hamiltonian, supplied with appropriate boundary conditions, also applies to the description of a single-mode field in an array of N evanescently coupled waveguides in the paraxial approximation. In this case, the amplitude of the transverse field on each waveguide becomes equivalent to the on-site amplitude of the wavefunction $|\psi\rangle$ in a solid state lattice. It the case of periodic boundary conditions (PBC) where $\psi_{N+1} = \psi_1$, $\psi_0 = \psi_N$, we take the corner matrix elements of the Hamiltonian of Eq. (2.1) as $\hat{H}_{N,0} = \hat{H}_{0,N} = 1$, while for open boundary conditions (OBC), where $\psi_{N+1} = \psi_0 = 0$, we take $\hat{H}_{N,0} = \hat{H}_{0,N} = 0$ instead. In the first case the waveguides are arranged in a linear chain, while in the second they form closed ring topology. We consider primarily a system with closed boundary conditions for this section; nonetheless, we remark that this system with periodic boundary conditions will not have a radically different behaviour for large system sizes N.

The Anderson tight-binding Hamiltonian ([1]) is a modification of the above such that the on-site potential is now a function of the site index n, taken at random from a rectangular probability distribution:

$$\epsilon_n \in [-W/2, W/2] \tag{2.3}$$

The system described by this Hamiltonian is not periodic and therefore Bloch's theorem no longer holds. The constant W is commonly called the disorder strength constant and determines how strongly localized the eigenstates are. To obtain the eigenstates and eigenvalues of such a system we use numerical exact diagonalization. The Anderson tight-binding Hamiltotian in this section is therefore given in matrix form as:

$$\hat{H} = \begin{pmatrix} \epsilon_1 & 1 & 0 & 0 & \dots & \delta \\ 1 & \epsilon_2 & 1 & 0 & \dots & 0 \\ 0 & \ddots & \ddots & \ddots & \dots & 0 \\ 0 & \dots & 1 & \epsilon_{N-2} & 1 & 0 \\ 0 & \dots & 0 & 1 & \epsilon_{N-1} & 1 \\ \delta & \dots & 0 & 0 & 1 & \epsilon_N \end{pmatrix} \tag{2.4}$$

where $\delta = 1$ for PBC and $\delta = 0$ for OBC.

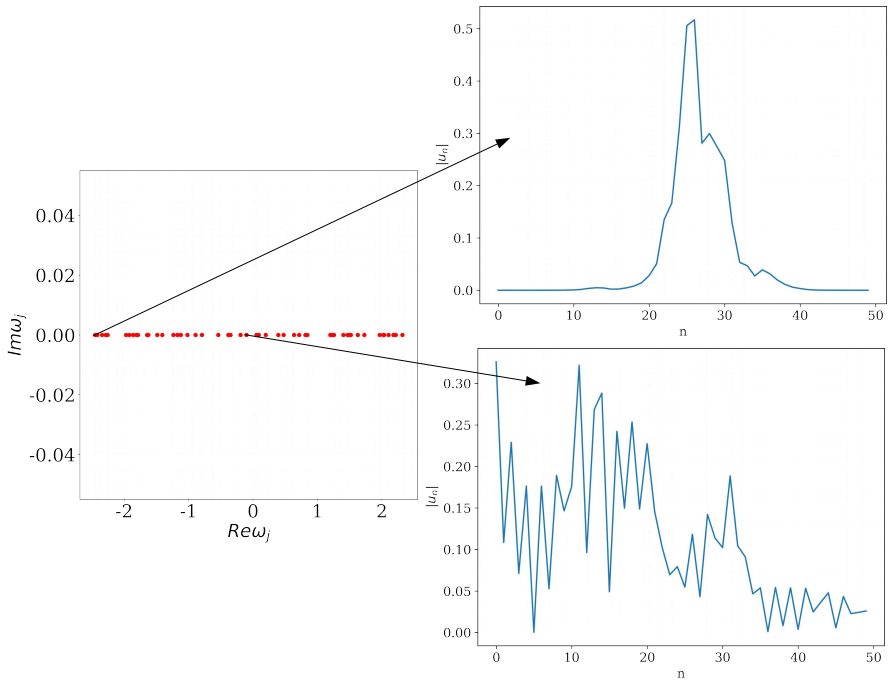

Figure 2.1: Example of two eigenstates $|u_j|$ in an Anderson lattice of size $N = 50$ with weak disorder ($W = 2$). A state with an eigenvalue on the center of the spectrum is localized, and decays exponentially in the region outside its localization site. On the contrary, a state with an eigenvalue around the center of the band extends to the whole lattice and behaves as an extended state (because $\xi_j > N$). In both cases, fluctuations can be observed in the wavefunction that dissipate as it extends to the rest of the lattice.

The one-dimensional Hamiltonian of Eq. (2.4) displays a spectral feature known as Anderson localization, wherein its eigenstates appear to be confined to a finite interval of the lattice and decay exponentially outside of it. A measure of this behavior is the localization length ξ. For an eigenstate $|u_j\rangle$ of this Hamiltonian, this behavior is qualitatively described by a relation of the form $|u_{jn}| \propto e^{-|n|/\xi_j}$ for n outside the area in which $|u_j\rangle$ is localized. The localization length ξ_j for each eigenstate is a function of its eigenvalue such that $\xi = \xi(\omega)$.

There are several numerical methods to determine the localization length associated with an eigenstate $|u\rangle_j$ for variable disorder strength W. The transfer matrix method ([9],[11]) considers an incident Bloch wave of frequency ω on the right side of an open lattice to determine the transmission coefficient. As the wave scatters through the disordered lattice, the decay factor in its amplitude for large n will give an estimate of the localization length. For such a wave, a recursive expression for ψ_n can be extracted from Eq. (2.2) as follows, by taking

$c = 1$:

$$(\omega - \epsilon_n)\psi_n = \psi_{n+1} + \psi_{n-1} \Rightarrow \psi_{n+1} = \frac{\omega - \epsilon_n}{\psi_n} - \psi_{n-1} \tag{2.5}$$

Then we obtain the system of equations:

$$\begin{bmatrix} \psi_{n+1} \\ \psi_n \end{bmatrix} = \begin{bmatrix} \omega - \epsilon_n & -1 \\ 1 & 0 \end{bmatrix} \begin{bmatrix} \psi_n \\ \psi_{n-1} \end{bmatrix} \equiv \hat{T}_n \begin{bmatrix} \psi_n \\ \psi_{n-1} \end{bmatrix} \tag{2.6}$$

where $\hat{T}_n$ is defined as the transfer matrix on the n-th site of the disordered lattice. This equation can be iterated by choosing $\psi_0^2 + \psi_1^2 \neq 0$ such that:

$$\begin{bmatrix} \psi_{n+1} \\ \psi_n \end{bmatrix} = (\prod_{j=1}^{n} \hat{T}_j) \begin{bmatrix} \psi_1 \\ \psi_0 \end{bmatrix} \tag{2.7}$$

Defining the Lyapunov exponent as $\gamma(\omega) = \lim_{n\to\infty} \ln(\psi_n^2 + \psi_{n+1}^2)$, the localization length is calculated as

$$\xi(\omega) = \frac{1}{\mathrm{Re}[\gamma(\omega)]} \tag{2.8}$$

which is consistent with the common definition of the localization length in one dimension as $\xi = -\lim_{n\to\infty} \frac{n}{\ln|\psi_n|}$.

After numerically diagonalizing the Hamiltonian of Eq. (2.4) for an Anderson lattice described by a random potential in the form of Eq. (2.3), Eq. (2.7) can be iterated over a large number sites for each eigenvalue ω_j in the spectrum. This process can then be repeated for an appropriate amount of realizations of disorder to obtain a converging average value of the localization length. To effectively determine the localization length in a disordered system using this technique, a large system size N is required, because the eigenstates tend to fluctuate significantly (Fig. 2.1) and thus require many consecutive iterations of the transfer matrix to achieve convergence. A more generalized method that employs the transfer matrix can be found in [9] and [10].

A simpler method that also takes into account the eigenstate solutions $|u_j\rangle$ is to perform a linear fit on each eigenstate of the form:

$$\ln|u_{jn}| \approx -\frac{1}{x_j}|m - n| + \text{intercept} \tag{2.9}$$

where m is the site for which $|u_{jn}|$ is maximum. In the case of OBC, this fit should be applied in both directions about the site m; in this case, the localization length can be determined by a weighted average of the slopes in the left and right directions:

$$\xi(\omega_j) = \frac{m\xi_j^L + (N - m)\xi_j^R}{N} \tag{2.10}$$

Repeating this process for many realizations of the Hamiltonian (2.4) for the same disorder strength W yields a set of eigenvalues which are then binned according to their magnitude. Averaging over all disorder realizations in each

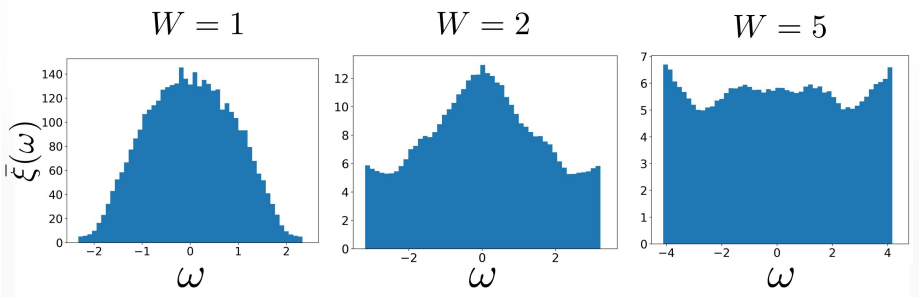

Figure 2.2: Average localization length $\bar{\xi}$ as a function of the eigenvalue ω for the eigenstates $|u\rangle$ of the Anderson tight-binding model described by Eqs. (2.1) and (2.3), calculated by linear regression on the eigenstate magnitude $|u_n|$ as a function of the site index n. The localization length was averaged over 200 realizations of disorder on a system size of $N = 500$ sites and over 50 bins, for $W = 1$, $W = 3$ and $W = 5$ (left to right). We can see that states with large $|\omega|$ are more strongly affected by the disorder.

bin will then give the average localization length for an interval in the spectrum of the system. The localization length calculated using this method for select values of the disorder strength W can be seen in Fig. 2.2.

In the case of a finite system and weak disorder strength, some eigenstates with eigenvalues about the center of the band may correspond to a localization length for which $\xi \gtrsim N$. In this case, the calculation for ξ will not necessarily converge and these eigenfunctions will behave as extended states for the system. Since the spectrum of this (finite) system is not completely localized, in contrast to the case of a system with strong disorder, transport may still take place; that is, an excitation at one end of the lattice will eventually reach the other end. For large system sizes we expect all states to be localized regardless.

We remark that in the context of the scaling theory of Anderson localization [6], this is not necessarily the case in higher dimensions. For two dimensional systems, there is a possibility that some states will behave as extended states even as $N \to \infty$, because the localization length corresponding to these states can be very large. For three dimensional systems and for a given disorder strength, the localization length diverges algebraically at a critical value of ω . For calculating the localization length of states that are not strongly localized, especially motivated by the study of two-dimensional systems, special computational methods have been developed beyond the naive approach used here, that can also be used in the case of weak disorder for one dimensional systems [12].

2.1.2 Absence of transport

To study the dynamics of the lattice described by the Anderson model of Eq. (2.2) in the context of photonics, we consider the set of equations concerning

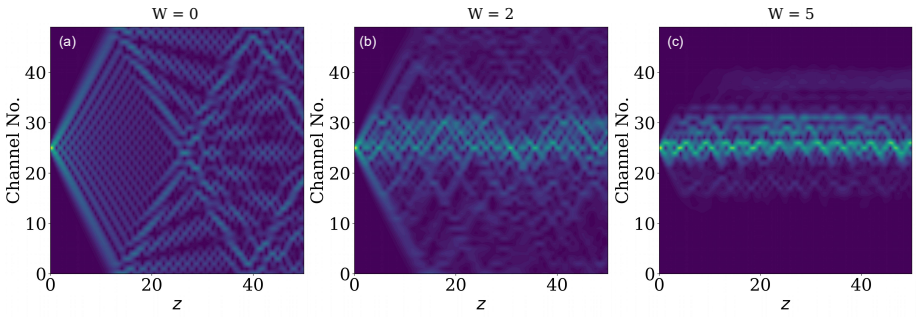

Figure 2.3: Evolution of a single channel excitation on the center of a lattice described by the Hamiltonian of equation (2.2) with closed boundary conditions, in the case of (a) no disorder (b) weak disorder and (c) strong disorder. In the last case, the disorder completely localizes the eigenstates; as such, no transport of the initial excitation outside a narrow area of the lattice is observed. Plotted is $|\psi_n|$ vs propagation distance z.

the propagation of the slowly varying component of the electric field $|\psi\rangle$ over propagation distance z in a one dimensional array of N evanescently coupled waveguides:

$$i\frac{\partial \psi_n}{\partial z} + \psi_{n+1} + \psi_{n-1} + \epsilon_n \psi_n = 0 \tag{2.11}$$

This evolution law for the propagation of light in multiple discrete channels is obtained via two approximations from the wave equation [13]. The first approximation is the paraxial approximation; by writing the electric field on each waveguide as $E_n(z) = u_n(z)\exp(ikz)$ and taking the field amplitude $\psi_n(z)$ to vary slowly with the propagation distance, such that we can neglect the second order derivative in z that appears in the wave equation, we obtain differential equations that are first order in z. The second is the tight binding approximation; because individual waveguides are close together their individual modes overlap, giving rise to coupling between neighboring waveguides. The evolution is then described by considering the self-energy ϵ_n on each site which depends on the local variation of the refractive index and the coupling constant c. Thus the field $|\psi\rangle$ describes the amplitude of the electric field in each waveguide site.

This set of equations is reminiscent of the time-dependent Schrödinger equation for wavefunctions in solid state tight binding lattices, with the propagation distance z appearing instead of the time t. The on-site potential can then be adjusted through the refractive index on each waveguide. It is important to note here that ϵ_n contains the difference of the local refractive index to the refractive index of the bulk material in which the array is contained; as such negative values for $\mathrm{Re}(\epsilon_n)$ do not physically correspond to backward propagating waves, and we may take the disorder distribution to be in a symmetric interval such as in Eq. (2.3).

The above system of N equations can be numerically integrated for any form of

ϵ_n, boundary and starting conditions by employing a 4th-order Runge-Kutta (RK) method over a discretized propagation interval $\{0, dz, 2dz, \ldots, (J-1)dz, Jdz\}$ with step dz. Then, writing the field in vectorized form as $|psi\rangle = (\psi_1\, \psi_2\, \ldots \psi_N)$, a step of the RK method starting at $z_j = jdz$ is performed as:

$$\begin{aligned}
|k_1\rangle &= i\hat{H}\,|\psi\rangle\,(z_j) \\
|k_2\rangle &= i\hat{H}\left(|\psi(z_j)\rangle + dz \cdot \frac{|k_1\rangle}{2}\right) \\
|k_3\rangle &= i\hat{H}\left(|\psi(z_j)\rangle + dz \cdot \frac{|k_2\rangle}{2}\right) \\
|k_4\rangle &= i\hat{H}\left(|\psi(z_j)\rangle + dz \cdot |k_3\rangle\right) \\
|\psi(z_{j+1})\rangle &= |\psi(z_j)\rangle + \frac{dz}{6}\left(|k_1\rangle + 2\,|k_2\rangle + 2\,|k_3\rangle + |k_4\rangle\right)
\end{aligned} \tag{2.12}$$

by observing that $\partial\,|\psi\rangle\,/\partial z = i\hat{H}\,|\psi\rangle$. This process is iterated for all $z_j = j \cdot dz$ where $j \in \{0, 1, 2, \ldots, J\}$ to finally get the field on the desired propagation distance z_{max}. In this work, 10^5 steps are used for determining the field up to propagation distances in the order of 10^2.

Another method that can be used to study the dynamics of the system involves the exponential matrix method. The evolution of the field $|\psi\rangle$ is given in terms of the evolution matrix $\hat{U}$ as:

$$|\psi(z)\rangle = \hat{U}(z)\,|\psi_0\rangle \equiv e^{i\hat{H}z}\,|\psi_0\rangle \tag{2.13}$$

where $|\psi_0\rangle$ is the initial field profile at $z = 0$. Then the same discretization as in the previous method can be employed to calculate the evolution matrix for a single step in the propagation interval as $\hat{U} = \exp(i\hat{H}dz)$. If dz is sufficiently small, the field $|\psi\rangle$ can then be calculated by iteratively multiplying with $\hat{U}$ as:

$$|\psi(z_{j+1)})\rangle = \hat{U}\,|\psi(z_j)\rangle \tag{2.14}$$

Both methods applied here yield similar results; the evolution matrix is more desirable in the case of systems where it is cumbersome to write down a RK method due to the complexity of the Hamiltonian $\hat{H}$. Because the tight-binding Hamiltonian involves only nearest neighbor coupling, here we choose to use the RK method.

The evolution of a field in the presence of strong disorder is limited to a small subsection of the lattice, in contrast to the ballistic transport of the field in the periodically ordered lattice [15]. As seen in Fig. 2.3, if the disorder strength W is large enough, the field does not reach the edges of the lattice - no transport is then observed.

2.2 Non-Hermitian disorder

2.2.1 Spectral properties and localization

We now consider the case of a system described by Eq. (2.2) with complex, rather than strictly real, random on-site potential ϵ_n. As in the case of the Anderson model, ϵ_n is drawn at random from a rectangular distribution as:

$$\mathrm{Re}(\epsilon_n) \in [-W_R/2, W_R/2],\ \mathrm{Im}(\epsilon_n) \in [-W_I/2, W_I/2] \tag{2.15}$$

In the case of an array of N coupled waveguides, the imaginary part of the on-site potential describes gain in the form of optical pumping ($\mathrm{Im}(\epsilon_n) < 0$) or losses in the form of cavity leaks and absorption by the waveguide material ($\mathrm{Im}(\epsilon_n) > 0$). The Hamiltonian of this system is no longer Hermitian, and therefore the norm of the field is not a conserved quantity of the lattice.

Since the Hamiltonian H is not self-adjoint, the (right) eigenvalue problem of Eq. (2.2) with complex disorder in the above form should be accompanied by the adjoint (left) eigenvalue problem of its Hermitian conjugate ($H^\dagger$); the two sets of right and left eigenstates satisfy the biorthogonality condition $\langle u_i^L | u_j^R \rangle = \delta_{i,j}$. The solutions of the right eigenvalue problem are complex eigenvalues ω_j and their associated eigenstates $|u_j\rangle$ that satisfy $\psi_j(z) = u_j^R e^{i\omega_j z}$ for the evolution of the complex field amplitude $\psi(z)$.

Writing down the two eigenvalue problems, it can be shown that the right and left eigenvalues and eigenstates are complex conjugates of one another, because the Hamiltonian remains symmetric ($\hat{H}^\dagger = \hat{H}^*$) ([47] - [48]):

$$\begin{cases} \hat{H}\,|u_j^R\rangle = \omega_j\,|u_j^R\rangle \\ \hat{H}^\dagger\,|u_j^L\rangle = \omega_j^*\,|u_j^L\rangle \end{cases} \Rightarrow \begin{cases} \hat{H}^*\,|u_j^R\rangle^* = \omega_j^*\,|u_j^R\rangle^* \\ \hat{H}^*\,|u_j^L\rangle = \omega_j^*\,|u_j^L\rangle \end{cases} \Rightarrow |u_j^R\rangle = |u_j^L\rangle^* \tag{2.16}$$

Therefore, for this system we only need to study the behavior of the right eigenstates (henceforth denoted simply as u_j) to obtain its dynamical and spectral properties. We may, furthermore, rule out the possibility of degenerate eigenstates by observing that the spectrum is determined by random diagonal elements.

To quantify the effect of the complex disorder on the spectrum of the system we may examine the distribution of the level spacings for the tight-binding Anderson model [48]. For a given realization of disorder, we denote the eigenvalues of the Anderson Hamiltonian by $\omega_{j,a}$, where a is the index corresponding to that specific realization. Since the distributions for the real and imaginary parts of the on-site potential ϵ_n are independent, we may restrict our study of the level spacings to the real part of the eigenvalues. Ordering the eigenvalues by descending order, the level spacings for a given realization are defined as:

$$s_{j,a} = \omega_{j,a} - \omega_{j+1,a} \tag{2.17}$$

To consider a statistical average over many realizations, we also define the normalized level spacings $\bar{s}_{j,a}$, which are defined as:

$$\bar{s}_{j,a} = \frac{s_{j,a}}{\langle s_{j,a} \rangle_a} \tag{2.18}$$

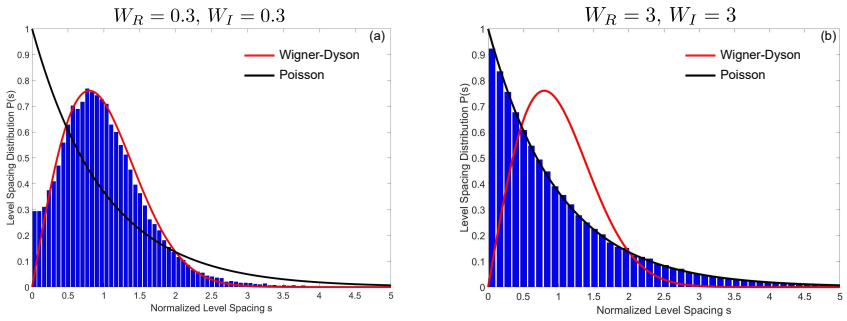

Figure 2.4: Distribution of the normalized level spacings $\bar{s}$ as defined by Eqs. (2.17) and (2.18) for the complex Anderson Hamiltonian defined by Eqs. (2.4) and (2.15). In both cases the normalized level spacings where calculated for a system of size $N = 1000$ over 50 realizations of disorder. (a) The distribution of the normalized level spacings for weak disorder $W_R = 0.3$, $W_I = 0.3$ is in agreement to that predicted by the Wigner-Dyson distribution of Eq. (2.19). (b) The distribution of the normalized level spacings for strong disorder $W_R = 3$, $W_I = 3$ is in agreement to that predicted by the Poisson distribution of Eq. (2.20).

where the notation $\langle \ldots \rangle_a$ denotes averaging over all realizations. For low values of the disorder strength W, the Anderson model is known to exhibit level repulsion, wherein the probability that there is an overlap between two eigenvalues tends to zero. The distribution of the normalized level spacings is then known to follow the Wigner-Dyson distribution [8]:

$$P_{WD}(\bar{s}) = \frac{\pi \bar{s}}{2} \exp(-\pi \bar{s}/4) \tag{2.19}$$

In the case of strong disorder, the effect of the level repulsion on the spectrum is diminished; the level spacings are determined by the random diagonal terms and as a result their distribution tends to the Poisson distribution:

$$P_P(\bar{s}) = \exp(-\bar{s}) \tag{2.20}$$

The results of this statistical analysis can be seen for two distinct cases of disorder in Figs. 2.4(a) and 2.4(b) for weak and strong disorder respectively. Between these two regimes there is an intermediate transition region where the effect of localization can be studied by considering the ratio between adjacent level spacings instead.

We then consider the effect of introducing gain or loss randomly on each site on the localization length; thus the disorder distribution describing our system in now non-Hermitian. Using the transfer matrix method outlined by Eq. (2.7), we calculate the localization length for variable disorder strength. For a potential drawn from a rectangle of sides W_R and W_I per Eq. (2.15) the system is described effective disorder strength which is given as $W_{\text{eff}} = \sqrt{W_R^2 + W_I^2}$. As seen in Fig. 2.5 in which the localization length is plotted alongside with the

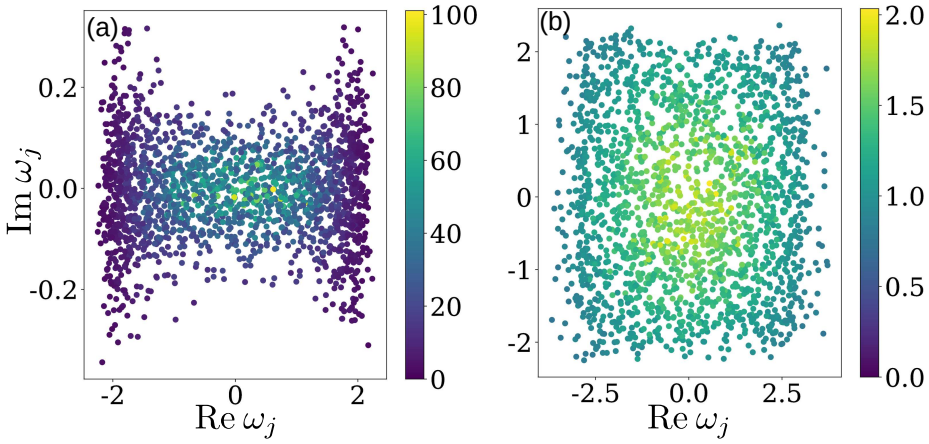

Figure 2.5: Spectra and localization length ξ (colorbar) plotted for the eigenstates of a non-Hermitian disordered lattice described by equations (2.1) and (2.15), (a) in the weak disorder ($W_R = W_I = 1$) and (b) in the strong disorder ($W_R = W_I = 5$) regimes. ($N = 500$, four realizations of disorder.)

eigenvalues in the complex plane, we have a similar behavior as in the Hermitian case [Fig. 2.2] where the localization length is greater for eigenvalues near the origin. In the case of weak disorder [Fig. 2.5a] the localization length for energies near the origin is in the order of magnitude of the system size, and therefore we do not have complete localization of the eigenstates. In contrast, in the case of strong disorder [Fig. 2.5(b)] all eigenstates are localized ($\xi \ll N$); in that case, the eigenstates span very few lattice sites before decaying as $\xi \sim 1$.

Another interesting feature of non-Hermitian systems is the non-orthogonality of the right eigenstates [48]. In the case of strong localization, the right eigenstates display some overlap with each other that depends on the strength of both the real and the imaginary parts of the disorder. To examine this feature, we sort the eigenstates $|u_j^R\rangle|$ by the index of their greatest n-component, thus arranging them by the order of the sites around which they are localized:

$$\text{argmax}(|u_{j,n}^R|) = j \Rightarrow \max(|u_j^R\rangle) = |u_{j,j}| \tag{2.21}$$

We may then define a "distance" s between two eigenstates $|u_j^R\rangle$ and $|u_i^R\rangle$ as the distance between the indices where each of the eigenstates is maximal as $s(|u_i^R\rangle, |u_j^R\rangle) = |i - j|$.

The average orthogonality of the right eigenstates is examined in Figs. 2.6(a-b), for variable disorder strengths W_I and W_R. In Fig. 2.6(a), the blue line corresponds to strong real and imaginary disorder, whereas the red line corresponds to weak imaginary disorder. In the second case, the eigenstates are still all localized, but because the strength of non-Hermiticity has decreased, immediately neighboring eigenstates have a smaller overlap. The black line

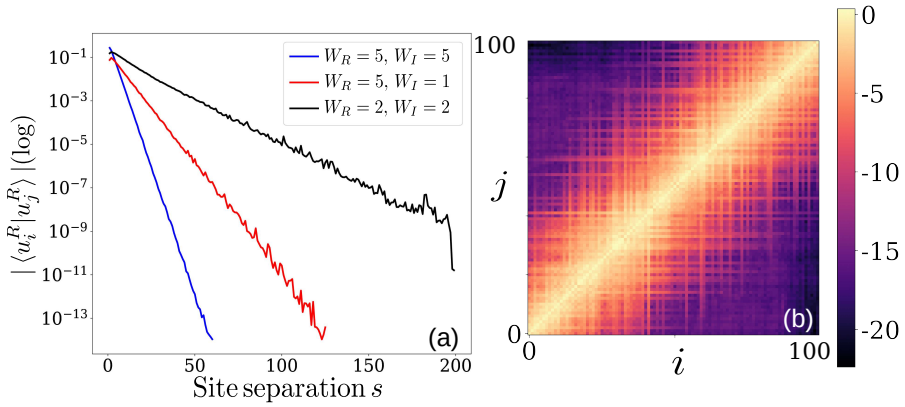

Figure 2.6: Orthogonality between right eigenstates for the Hamiltonian described by Eqs. (2.2) and (2.15). (a) Orthogonality between eigenstates localized around sites separated by distance s, for various disorder strengths , averaged over 20 realizations ($N = 200$). Between neighboring localized eigenstates ($s = 1$), the overlap is smaller for weaker imaginary part disorder (the non-Hermiticity is reduced). (b) Orthogonality matrix (log scale, colorbar) for the right eigenstates of a lattice with $N = 100$ sites under strong disorder ($W_R = 5, W_I = 5$) as a function of eigenstate sites. The overlaps decrease exponentially as s increases.

corresponds to weak complex disorder; while extended states are present, the overlap still decreases for distant eigenstates. In all cases, the magnitude of the overlap for eigenstates localized around neighboring sites is in the order of 10^{-1}, and it decreases exponentially as s increases. The rate of the exponential decrease depends on the localization length of the eigenstates which in turn depends on the effective strength of the disorder.

This exponential decrease can be confirmed to hold individually in the case of strong disorder by examining the orthogonality matrix of the right eigenstates [Fig. 2.6(b)]. It is not expected to consistently hold in the case of a lattice with weak complex disorder (where there are many extended eigenstates). In all cases, the exponential decrease of the overlap indicates that non-orthogonality is not a feature that greatly determines the dynamics of the non-Hermitian Anderson model.

2.2.2 Dynamics and delocalization via jumps

We now turn our attention to the dynamics of a non-Hermitian Anderson lattice. We first note that because the eigenvalues are complex, each eigenstate evolves as $|u_j\rangle(z) = |u_j\rangle e^{(i\mathrm{Re}\omega_j - \mathrm{Im}\omega_j)z}$, and therefore its magnitude either diverges exponentially or vanishes as the propagation distance z increases. Because in principle a single channel excitation excites all eigenstates of the system, this implies that in general the most gainy states will dominate the dynamics for

large values of z. As a result, we expect to find the field $|\psi\rangle(z)$ in the eigenstate with the greatest negative imaginary part for large propagation distances.

We also consider the optical power of $|\psi\rangle$ as

$$\mathcal{P}(z) = \sum_{n=1}^{N} |\psi_n(z)|^2 \tag{2.22}$$

For a Hermitian lattice, $\mathcal{P}(z)$ is one of the conserved quantities; for a non-Hermitian system, the optical power $\mathcal{P}(z)$ varies with z. The optical power $\mathcal{P}(z)$ has the same divergent behavior as $|\psi(z)\rangle$, where it increases exponential if any gainy eigenstates are present in the spectrum.

To mitigate this divergence, we consider the normalized field $|\phi(z)\rangle \equiv \frac{|\psi(z)\rangle}{\sqrt{\mathcal{P}(z)}}$, for which the power is by definition $\mathcal{P}_\phi(z) = 1\,\forall z$. Then we rewrite Eq. (2.11) for the normalized field $|\phi(z)\rangle$ as:

$$i\frac{\partial \phi_n}{\partial z} + \phi_{n+1} + \phi_{n-1} + \epsilon'_n(z)\phi_n = 0 \tag{2.23}$$

where $\epsilon'_n(z) = \epsilon_n + \frac{i}{2}\frac{d\ln\mathcal{P}(z)}{dz}$ is the new z-dependent on-site potential derived by substituting the field into equation (2.11). This new quantity illustrates that the rate of gain/loss is significant in determining how the "center of mass" of the field will propagate through the lattice.

To study the dynamics of the field we employ the RK method of Eq. (2.12) with an additional normalization step. Because of the normalization we obtain effectively the dynamics for $|\phi(z)\rangle$ instead $|\psi(z)\rangle$. The normalization step is performed on the end of each step as:

$$\begin{aligned} |\phi(z_{j+1})\rangle &\leftarrow \frac{|\psi(z_{j+1})\rangle}{\sqrt{\sum_{n=1}^{N}|\psi_n(z_{j+1})|^2}} \\ P_{j+1} &\leftarrow \sum_{n=1}^{N}|\psi_n(z_{j+1})|^2 \\ |\psi(z_{j+1})\rangle &\leftarrow |\phi(z_{j+1})\rangle \end{aligned} \tag{2.24}$$

This extra step allows for the calculation of normalized field in the case where numerical overflows would prevent the calculation of $|\psi(z)\rangle$. The power can then be retrieved by a cumulative multiplication for $z_i = i \cdot dz$ as $\mathcal{P}(z_i) = \prod_{j=0}^{i} P_j$, with P_j defined above, and similarly the physical field $|\psi\rangle$ is recovered as $|\psi(z_j)\rangle = |\phi(z_j)\rangle \cdot \prod_{i=0}^{j}\sqrt{P_j}$.

We now consider the evolution of single-channel excitation in a non-Hermitian lattice in the strong disorder regime ($W_R = W_I = 5$), as seen in Fig. 2.7. Initially, the initial excitation is transported only a small region around the excitation channel inside of which the field remains localized. However, a new and interesting effect is exhibited by the evolution of the initial excitation in the appearance of sudden "jumps" between distant lattice sites, representing a change in the localization site of the field.

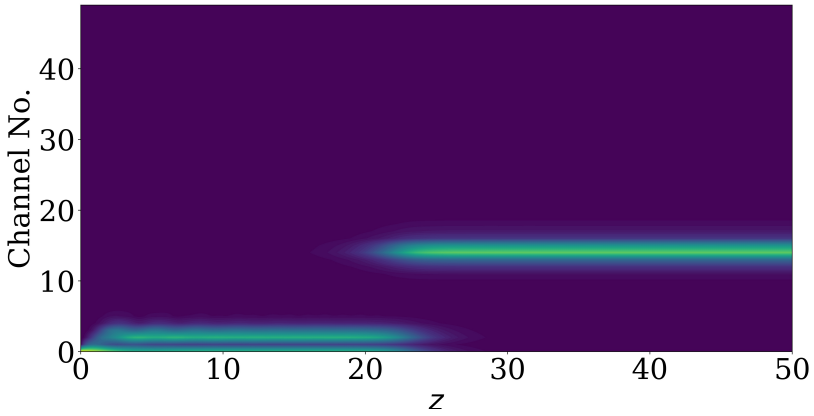

Figure 2.7: Evolution of the normalized field $|\phi_n|$ for a single channel excitation in a non-Hermitian lattice described by Eqs. (2.11) and (2.15) and closed boundary conditions. While the field is evidently localized, a sudden jump appears around $z = 25$ that represents a sudden shift in the field's center of mass.

Because the distribution of gain and loss governed by Eq. (2.15) is even, this effect initially seems to be caused by the selective amplification of the field on select sites realized in the form of optical pumping. While the absence of transport in the case of 1D disordered lattices has been well studied in the context of Anderson localization, the introduction of non-Hermitian terms in disordered systems has been shown to introduce new delocalization effects in the form of quantized "jumps" ([58] - [59]), implying the suppression of Anderson localization for certain non-Hermitian systems. To avoid considering external supply of energy as a factor which affects propagation, we consider an alternative "uneven" distribution of non-Hermitian disorder which features only loss on each site:

$$\mathrm{Re}(\epsilon_n) \in [-W_R/2, W_R/2]\,, \mathrm{Im}(\epsilon_n) \in [0, W_I] \tag{2.25}$$

Remarkably, a lattice with only losses also displays the effect of jumpy propagation, as seen in Fig. 2.8(a), showing that delocalization via jumps is not an effect of amplification, but a consequence of the complex spectrum introduced via the non-Hermitian disorder term. Furthermore, since delocalization via jumps appears in the strong disorder regime, it also cannot be explained by transport of the initial excitation via extended eigenstates, because all eigenstates are localized. To better study the effect of the loss on the propagation profile, we expand the on-site field amplitude ψ_n in a linear combination of the right eigenstates as:

$$\psi_n = \sum_{j=1}^{N} c_j u_{jn} \tag{2.26}$$

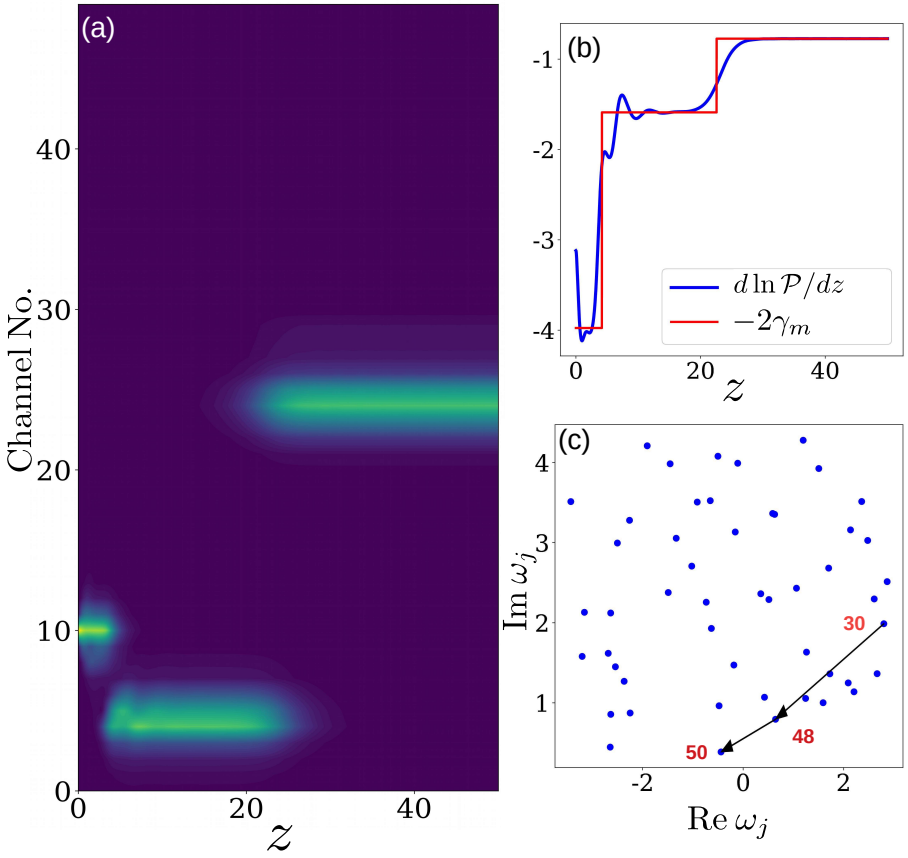

Figure 2.8: Dynamics and spectrum for a non-Hermitian lattice of size $N = 50$ described by Eqs. (2.2) and (2.25), with strong disorder ($W_R = W_I = 5$) and closed boundary conditions. (a) Evolution of the normalized field $|\phi_n|$ for a single-channel excitation placed on $n = 10$. Distinctive jumps take place at $z = 5$ and $z = 25$. Between two consecutive jumps, a single mode dominates the power derivative. (b) The derivative of the power logarithm by considering all modes (blue line) compared to its decay considering only the most dominant mode on each interval. The jumps are evident here as well. (c) Spectrum in the complex plane. The labeled eigenvalues (sorted by decreasing imaginary part) denote the dominant modes on each interval, and the arrows that connect them the transition that is associated with each jump.

where $c_j = \langle u_j^L|\psi\rangle$ is the projection coefficient of the field on the j-th right eigenstate. Denoting $\mathrm{Im}\,\omega_j = \gamma_j$ for the eigenvalues, we find that:

$$i\frac{d|c_j|^2}{dz} = i\frac{dc_j}{dz}c_j^* + i\frac{dc_j^*}{dz}c_j = -(\omega_j - \omega_j^*)|c_j|^2 = -2\gamma_j|c_j|^2 \Rightarrow |c_j| = e^{-\gamma_j z}|c_j|_{(z=0)} \tag{2.27}$$

using that a left eigenstate evolves as $|u_j^L(z)\rangle = e^{-i\omega_j^* z}\,|u_j^L\rangle_{(z=0)}$. Then by using the expansion of the field in right eigenstates, we can obtain a modal form for the optical power $\mathcal{P}(z)$ of the field:

$$\mathcal{P}(z) = \sum_{n=1}^{N}\sum_{i,j=1}^{N}(c_i u_{in})(c_j u_{jn})^* = \sum_{i,j=1}^{N} c_i c_j^* \Gamma_{i,j} \tag{2.28}$$

using that $\sum_{n=1}^{N} u_{in}u_{jn}^* \equiv \langle u_j^R|u_i^R\rangle \equiv \Gamma_{i,j}$ is overlap between the right eigenstates $|u_j^R\rangle$ and $|u_i^R\rangle$ that appears in the orthogonality matrix $(\Gamma)_{ij}$. At this point we can use the numerical results presented in Figs. 2.6(a) and 2.6(b); in the strong disorder regime, we can approximate the orthogonality matrix by only considering its diagonal, and therefore arriving at an "almost-orthogonal" approximation:

$$\Gamma_{i,j} = \delta_{i,j}\Gamma_{j,j} \tag{2.29}$$

Per Eq. (2.23), the quantity that chiefly determines the potential and the dynamics of the normalized field is the derivative of power logarithm. Using the above approximation regarding right eigenstate orthogonality, we may derive approximate expressions for this quantity for various forms of the field profile. Our results are shown in Figs. 2.8 and 2.9 for the dynamics of the normalized field $|\phi\rangle$ considering an initial single-channel excitation on an Anderson lattice with open boundary conditions and only loss.

Considering initially the case where a single mode $|u_m^R\rangle$ (with respective eigenvalue ω_m) dominates the field profile (such as $c_j \ll c_m$ for all other modes $|u_j^R\rangle$ with $j \neq m$), we may derive approximate for $\frac{d\ln\mathcal{P}}{dz}$ that:

$$\ln\mathcal{P}(z) \approx \ln\sum_{j=1}^{N}|c_j|^2\Gamma_{j,j} \approx \ln(|c_m|^2_{z=0}\Gamma_{m,m}) - 2\gamma_m z \Rightarrow \frac{d\ln\mathcal{P}(z)}{dz} = -2\gamma_m \tag{2.30}$$

This explains the flat sections in the derivative of the power logarithm seen in Fig. 2.8(b), which correspond to the intervals between two consecutive jumps in the dynamics of $|\phi\rangle$.

We may also derive the sigmoid transition in the power logarithm derivative for two competing modes $|u_n^R\rangle$ and $|u_m^R\rangle$ with corresponding amplification/dissipation rates $\gamma_m < \gamma_n$, by considering a case where $|c_n| \gg |c_j|$, $|c_m| \gg |c_j|$ for all $j \neq m, n$ in an interval $[z_1, z_2]$ where the jump takes place. Using only the approximation for the orthogonality matrix of the right eigenstates, we can obtain the following expression for the power derivative:

$$\frac{d\ln\mathcal{P}(z)}{dz} = \frac{\sum_{j=1}^{N} -2\gamma_j A_j e^{-2\gamma_j z}}{\sum_{j=1}^{N} A_j e^{-2\gamma_j z}} = -2\gamma_n\frac{1 + \sum_{j\neq n}\frac{\gamma_j}{\gamma_n}\frac{A_j}{A_n}e^{-2(\gamma_j-\gamma_n)z}}{1 + \sum_{j\neq n}\frac{A_j}{A_n}e^{-2(\gamma_j-\gamma_n)z}} \tag{2.31}$$

where $A_j \equiv |c_j|^2_{z=0}\Gamma_{j,j}$, and u_n is assumed to be dominant at $z_1 = 0$ (for simplification purposes). Then we may ignore other terms in the sum and obtain:

$$\frac{d\ln\mathcal{P}(z)}{dz} = \frac{-2\gamma_n}{1+\frac{A_m}{A_n}e^{-2(\gamma_m-\gamma_n)z}} + \frac{-2\gamma_m\frac{A_m}{A_n}e^{-2(\gamma_m-\gamma_n)z}}{1+\frac{A_m}{A_n}e^{-2(\gamma_m-\gamma_n)z}} \tag{2.32}$$

In the case that $\gamma_m < \gamma_n$, the left term vanishes as the propagation distance increases and the right term describes a sigmoid curve that connects the two consecutive intervals where $|u_n^R\rangle$ and $|u_m^R\rangle$ are dominant. This feature is clearly observed in the last jump in Fig. 2.8(b).

We stress that the above analytical approximations are valid in the case of strong disorder, where the overlaps between the right eigenstates decay exponentially and the orthogonality matrix can be approximated by its diagonal. In this case, the "trajectory" of the jumps is determined by the magnitude of the projection coefficients of the field amplitude on the right eigenstates $|c_j|$. To determine the propagation distance z where a jumps takes place, and therefore which mode is dominant on each interval, we plot $\ln|c_j|$ versus z (Fig. 2.9(a)). The jumps can then be predicted by examining how competing modes overtake each other as their projection coefficients evolve.

Our results using the analysis outlined in this section are outlined in Figs. 2.9(a-b). The line indices correspond to the indices of the modes sorted by in ascending order by decreasing imaginary part of their eigenvalues (from most to least lossy in this case). The blue, orange and green lines (modes 30, 48,50) correspond to modes that are dominant in each interval between the jumps seen in Figs. 2.8(a) and 2.8(b); in the interval in which each of these mode is dominant the corresponding line is accented. The crossings of these lines predict exactly the point where one mode overtakes another and therefore the position of each jump (at $z \sim 5, 25$). Since the slopes of the lines are determined by the corresponding decay rate γ_j, the dynamics and positions of the jumps are determined by the initial values of the projection coefficients (the intercepts of the lines). While modes 40 and 49 (intermittently dashed and doted lines) decay slower than the previous dominant modes 30 and 48 respectively, there are no jumps to these modes; for mode 49, the reason is the small value of its initial projection coefficient. For mode 40, the critical factor for its non-participation in jumps is the high value of its decay rate.

Furthermore, the analytical approximations of Eqs. (2.30) and (2.32) outlined in this section as seen in Fig. 2.9(a) are in excellent agreement with the exact dynamics presented in Fig. 2.8(a-b), and predict correctly the trajectory of the light in the complex eigenvalue plane depicted in Fig. 2.8(c).

2.2.3 Eigenvalue shifting for the normalized field

Another way to study the dynamics of delocalization via jumps is to examine how the eigenvalues $\tilde{\omega_j}(z)$ of the normalized field Hamiltonian (defined from Eq. (2.23)) shift in the complex plane as the propagation distance z increases and the optical power $\mathcal{P}(z)$ evolves. Because the on-site potential ϵ_n' of the modified Eq.

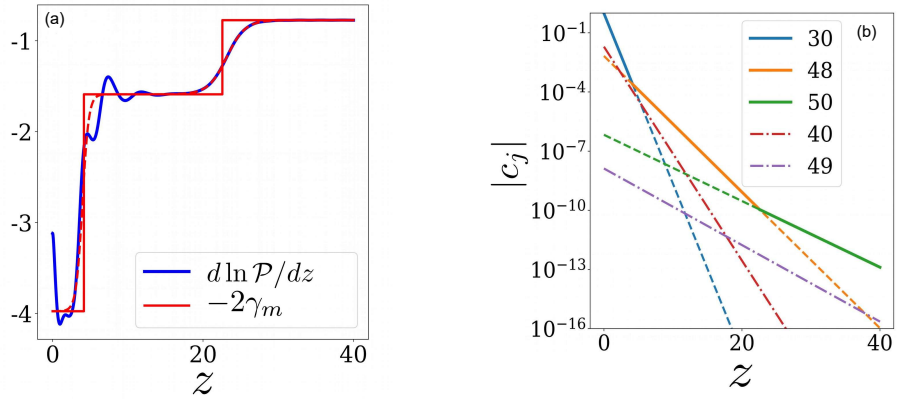

Figure 2.9: (a) Derivative of the power logarithm for the dynamics in Figs. (2.8)(a-c). The exact evolution of the optical power (blue curve) is predicted accurately by both the single dominant mode approximation of Eq. (2.30) (red discontinuous lines) and the sigmoid approximation of Eq. (2.32) (continuous dashed red line). (b)Magnitude of the projection coefficients $|c_j|$ (log scale) for the fields dynamics in Figs. 2.8(a-c). Lines 30, 48 and 50 correspond to the dominant modes; the crossings of these lines determine the position of the jumps.

(2.23) differs from ϵ_n by a power-dependent diagonal term, the eigenstates of both Hamiltonians are the same and the eigenvalues of the modified Hamiltonian differ by those of that of Eq. (2.2) by the same term:

$$\tilde{\omega_j}(z) = \omega_j + \frac{i}{2}\frac{d\ln\mathcal{P}(z)}{dz} \equiv \tilde{\omega_j}(0) + \frac{i}{2}\frac{d\ln\mathcal{P}(z)}{dz} \tag{2.33}$$

Therefore, when a single mode u_m is dominant at $z = z_1$ and the approximation (2.30) holds, we expect that:

$$\tilde{\omega_m}(z_1) = \mathrm{Re}\omega_m + i\gamma_m + \frac{i}{2}\frac{d\ln\mathcal{P}(z)}{dz}|_{z=z_1} \simeq \mathrm{Re}\omega_m + i\gamma_m - i\gamma_m = \mathrm{Re}\omega_m \tag{2.34}$$

Therefore $|u_m^R\rangle$ for the normalized field behaves as a state without loss or gain when it is dominant. This implies that for the normalized field to have constant power (by definition), all other eigenstates must either be occupied in such a way as to balance loss and gain or not occupied at all (condition on saturation). Regarding the asymptotic behavior of the model at large values of z, after the last jump has take place, all eigenvalues for the modified Hamiltonian of the normalized field correspond to lossy eigenstates without any energy content, except for the eigenvalue of the least lossy/most gainy state $|u_m^R\rangle$ for which $\mathrm{Im}(\tilde{\omega}_m) \to 0$ (see Fig. 2.10). This is consistent with the exponential evolution of the projection coefficients $|c_j|$ which predicts that on saturation only one mode is significantly occupied, and the power derivative curve of Fig. 2.9(a).

The explanation given for the appearance of jumps, and the analytical expressions derived, are expected to hold in the case of strong disorder. In

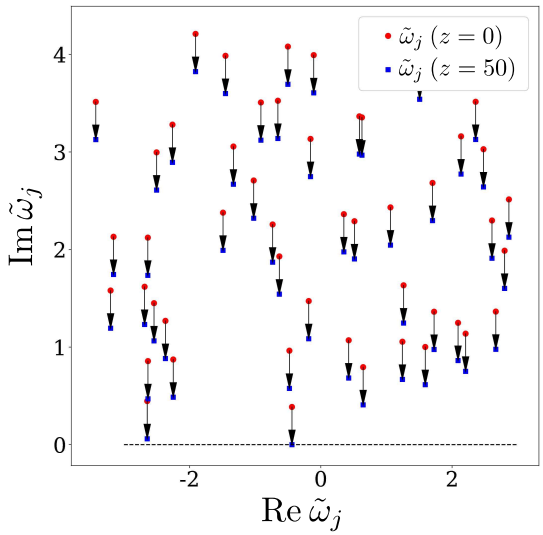

Figure 2.10: Shifting of the eigenvalues of the Hamiltonian for the normalized field defined by Eq. (2.23) for the same realization and initial conditions as in Fig. 2.8(a). The asymptotic behavior of the normalized field is $|\phi\rangle \to |u_m^R\rangle$ for large values of z, where $|u_m\rangle$ is the least lossy mode. For this mode $\mathrm{Im}(\tilde{\omega_m})) \to 0$, which is consistent with the norm of the normalized field $|\phi\rangle$remaining constant. Every other mode becomes lossy $(\mathrm{Im}(\tilde{\omega}_{j\neq m}) > 0)$.

the case the effective disorder of Eq. (2.15) is weak, the presence of extended eigenstates in the spectrum will decrease the rate of exponential decay of the overlaps that as seen in Fig. 2.6(a); therefore, the first approximation in (2.30) about the orthogonality of the right eigenstates will no longer be correct, and terms that involve the overlap of different eigenstates must be included when determining the form of the power logarithm derivative.

In practice, however, the extended states that appear correspond to eigenvalues that are located within a radius about the origin, similarly to the Hermitian case of weak disorder [Fig. 2.1]. Therefore, even in the case of weak disorder, the possibility of strongly localized eigenstates with strong amplification $(\mathrm{Im}(\omega) \sim -W_I/2)$ or dissipation $(\mathrm{Im}\,(\omega) \sim W_I/2)$ still remains, as seen in Fig. 2.5(a). In this case, if the field becomes localized in such a mode, jumps may still occur if the prerequisites in Eq. (2.32) are fulfilled. An alternative case is that the field transports until it becomes localized in the most gainy/least lossy mode; in this case saturation is reached without delocalization via jumps.

In the case of strong real disorder and weak imaginary disorder, jumps are expected to occur as the prerequisites for the approximation (2.30) are fulfilled; however because amplification and/or dissipation effects are weak, jumps in this case will take place over larger propagation distances.

2.3 Summary and discussion

The case of the Anderson model with the addition of a non-Hermitian random on-site potential term is associated with the appearance of a form of delocalization via jumps in the dynamics of the system, that does not appear in the Hermitian case [cf. Figs. 2.3(c) and 2.7]. The jumps can be predicted in the strong disorder regime by expanding the field in a linear combination of the right eigenstates using the biorthogonality condition [Eq. (2.16)] and calculating the projection coefficient for each eigenstate [Eq. (2.26)]. By taking the right eigenstates to be approximately orthogonal, we then derive an expression for the power logarithm derivative [Eqs. (2.27)-(2.32)], which characterizes the dynamics of the system for the normalized field [Eq. (2.23)]. Our analysis appears to hold best in the case of strong disorder where the almost orthogonal approximation of Eq. (2.29) for the orthogonality matrix of the right eigenstates is valid, as seen in Figs. 2.6(a)-(b).

Chapter 3

The Hatano-Nelson model

The results of the previous chapter indicate that the appearance of jumps is an effect that originates from the interaction of disorder and non-Hermiticity in the dynamics of a random lattice. Based in this discussion, one would expect that jumpy dynamics are always present in non-Hermitian disordered models. To examine if this is valid, we turn our attention to the well-studied assymetric Hatano-Nelson model ([60] - [62]), which is described by a tight-binding Hamiltonian with non-reciprocal off-diagonal coupling elements:

$$\hat{H}_{HN} = \sum_{n=1}^{N} \epsilon_n |n\rangle \langle n| + \sum_{n=1}^{N} \left[e^{-h} |n\rangle \langle n+1| + e^{h} |n\rangle \langle n-1| \right] \tag{3.1}$$

where h is a real constant and ϵ_n is the on-site potential that can either be constant, periodic or in the form of Eq. (2.15), as in the disorder term of the Anderson model. The Hatano-Nelson model can be implemented in a photonic lattice using non-reciprocal waveguides. The summation of the coupling terms takes into account the boundary conditions; for OBC $|0\rangle = |N+1\rangle = 0$, while for PBC $|0\rangle = |N\rangle$, $|N+1\rangle = |0\rangle$. Because the real off-diagonal matrices are not equal, this model is non-Hermitian. Furthermore, the choice $h \neq 0$ introduces a preferred direction of propagation to the left ($h < 0$) or the right ($h > 0$); in contrast to the ballistic transport in the case of a tight-binding Hermitian lattice, an excitation does not propagate uniformly in both directions [63].

In contrast to non-Hermitian tight-binding models, the system of Eq. (3.1) displays radically different dynamical and spectral properties depending on the choice of boundary conditions, as we will see in this section. This effect is known as the non-Hermitian skin effect, which has been studied extensively for this model as well as more generally for non-Hermitian lattices in one ([67] - [68]) or more ([69] - [71]) spatial dimensions.

3.1 The periodic Hatano-Nelson model

To understand the effect of real diagonal disorder on the spectral and dynamical properties of the Hatano-Nelson model, it is instructive to examine a case without disorder. To that effect, we take a finite system of N non-reciprocal waveguides, the dynamics of which are described by a system of N differential equations:

$$i\frac{\partial \psi_n}{dz} + e^{h}\psi_{n-1} + e^{-h}\psi_{n+1} = 0 \tag{3.2}$$

where $\epsilon_n = 0\,\forall n$ in Eq. (3.1). We should examine the spectrum of this system for both choices of boundary conditions. We first examine the case of OBC by taking $\psi_0 = \psi_{N+1} = 0$. In this case, the Hatano-Nelson Hamiltonian becomes a tridiagonal non-Hermitian matrix:

$$\hat{H}_{OBC} = \begin{bmatrix} 0 & e^{-h} & 0 & 0 & \dots & 0 \\ e^{h} & 0 & e^{-h} & 0 & \dots & 0 \\ 0 & e^{h} & 0 & \ddots & \dots & 0 \\ \vdots & \vdots & \ddots & \ddots & \ddots & \vdots \\ 0 & 0 & \dots & e^{h} & 0 & e^{-h} \\ 0 & 0 & \dots & \dots & e^{h} & 0 \end{bmatrix} \tag{3.3}$$

The Hamiltonian of Eq. (3.3) can be solved by considering an imaginary gauge transformation for the components of the field ψ_n on each site, such that $\tilde{\psi}_n = e^{-hn}\psi_n$ [61]. Then the system of Eqs. (3.2) can be rewritten as:

$$\begin{aligned} &i\frac{\partial \tilde{\psi}_n}{dz}e^{hn} + e^{h}e^{h(n-1)}\tilde{\psi}_{n-1} + e^{-h}e^{h(n+1)}\tilde{\psi}_{n+1} = 0 \Rightarrow \\ &i\frac{\partial \tilde{\psi}_n}{\partial z} + \tilde{\psi}_{n+1} + \tilde{\psi}_{n-1} = 0 \end{aligned} \tag{3.4}$$

In this orthogonal but not normal basis, the eigenvalues of $\hat{H}_{OBC}$ are identical to those of the Hamiltonian of Eq. (2.1) describing a periodic Hermitian lattice with OBC, and therefore are all real and independent of h. Then, denoting the eigenstates of Eq. (2.1) with OBC as $|u_j^R\rangle$, the eigenstates of the OBC Hatano-Nelson Hamiltonian are then written as $\psi_{n,j}^R = u_{j,n}^R e^{i\omega_j z}e^{-hn}$, while the left eigenstates (which can be found in the same manner for $h \to -h$) are then written as $\psi_{n,j}^L = u_{j,n}^L e^{i\omega_j^* z}e^{hn}$. The right eigenstates then take the appearance of edge states concentrated on the right or left side of the lattice, depending on the sign of h. Each left eigenstate $|u_j^L\rangle$ is related to $|u_j^R\rangle$ by $u_{j,n}^L = e^{-2hn}u_{j,n}^R$; the left eigenstates appear as edge states localized on the opposite site of the lattice to the right eigenstates.

To better understand the dynamics of the Hatano-Nelson model in the case of closed boundary conditions, we briefly examine an exactly solvable case of Eq. (3.3) for $N = 3$ (Fig. 3.1). For initial conditions, we consider an excitation

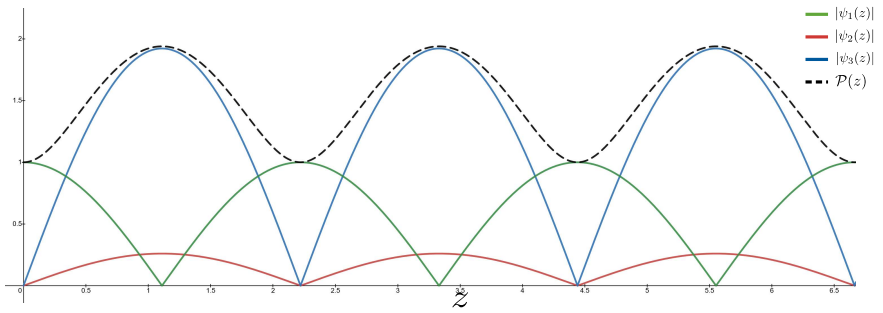

Figure 3.1: Example of the dynamics of Hatano-Nelson lattice with $N = 3$ and closed boundary conditions, for a single channel excitation on $n = 2$ and $h = 1$. The power of field and the field amplitude on each channel are all periodic functions (3 periods are plotted.)

on the center of the lattice $n = 2$. Then, the following initial conditions for the derivatives of the field amplitudes ψ_n can be derived:

$$\frac{\partial\psi_1}{dz} = ie^{-h},\ \frac{\partial\psi_3}{dz} = ie^{h},\ \frac{\partial\psi_2}{dz} = 0\ (\text{at } z = 0) \tag{3.5}$$

From these expressions we expect to observe asymmetric transport in one direction of the lattice (specifically to the right in the case that $h > 0$) [64]. The solutions for the field amplitude on each site for the $N = 3$ are:

$$\begin{aligned}\psi_1(z) &= i\frac{e^{-h}}{2}\sin(\sqrt{2}z)\\ \psi_2(z) &= \cos(\sqrt{2}z)\\ \psi_3(z) &= i\frac{e^{h}}{2}\sin(\sqrt{2}z)\end{aligned} \tag{3.6}$$

which indicate that the center of mass of field $\psi(z)$ oscillates between the center and right channels for $h > 0$. As such, there is only gainy propagation: the power of $\psi(z)$ oscillates between 1 and $\sqrt{\cosh(2h)} \geq 1$. Lossy propagation is only possible in the case of an excitation on the rightmost ($h > 0$) or the leftmost ($h < 0$) site of the lattice. This oscillatory behavior (which also applies to larger lattices) also predicts the lack of gainy or lossy modes for the OBC Hatano-Nelson model. At this point we stress that even if the spectrum of a non-Hermitian system is real, the optical power $\mathcal{P}(z)$ remains a non-conserved quantity; the reality of the spectrum however implies that averaged over large propagation distances there is no net gain or loss. The underlying reason for the oscillatory evolution of the optical power is the non-orthogonality of the right eigenstates, which is always a feature of non-Hermitian systems.

In the case periodic boundary conditions, the spectral and dynamical properties of the system are radically different. By applying the gauge transformation

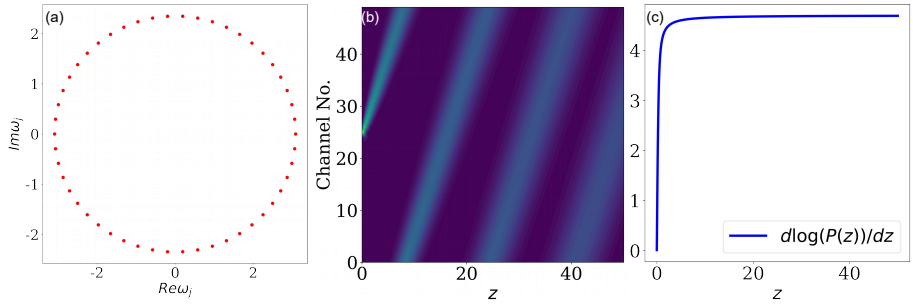

Figure 3.2: Features of the periodic Hatano-Nelson model with periodic boundary conditions, in a lattice with $N = 50$ and $h = 1$. (a) Elliptical spectrum in the complex plane. (b) Dynamics of a single channel excitation in the middle of the lattice, for the normalized field $|\phi_n|$, as defined in the previous chapter. The center of mass of the normalized field moves uninhibited to the right. (c) The power derivative for the propagation in (a): note that the field is amplified at a steady rate after the left propagating wave has dissipated.

as in the OBC case, the Hatano-Nelson Hamiltonian for periodic boundary conditions becomes:

$$\hat{H}_{PBC} = \begin{bmatrix} 0 & e^{-h} & 0 & 0 & \dots & e^{h} \\ e^{h} & 0 & e^{-h} & 0 & \dots & 0 \\ 0 & e^{h} & 0 & \ddots & \dots & 0 \\ \vdots & \vdots & \ddots & \ddots & \ddots & \vdots \\ 0 & 0 & \dots & e^{h} & 0 & e^{-h} \\ e^{-h} & 0 & \dots & \dots & e^{h} & 0 \end{bmatrix} \Rightarrow$$

$$\hat{\tilde{H}}_{PBC} = \begin{bmatrix} 0 & 1 & 0 & 0 & \dots & e^{hN} \\ 1 & 0 & 1 & 0 & \dots & 0 \\ 0 & 1 & 0 & \ddots & \dots & 0 \\ \vdots & \vdots & \ddots & \ddots & \ddots & \vdots \\ 0 & 0 & \dots & 1 & 0 & 1 \\ e^{-hN} & 0 & \dots & \dots & 1 & 0 \end{bmatrix}_{N\times N} \tag{3.7}$$

where $\hat{\tilde{H}}_{PBC}$ is the Hamiltonian in the $\tilde{\psi}_n$ basis, which remains non-Hermitian. For this reason, the eigenvalues are complex and they depend on the parameter h. This extreme sensitivity of the spectrum on the boundary conditions is characteristic of non-Hermitian systems, known as the non-Hermitian skin effect (NHSE) ([65]-[68]). In this case, the effect describes the sudden transition from extended complex eigenstates (PBC) to real edge states (OBC) and the collase of the eigenvalue spectrum to the real axis.

The eigenvalues of the Hatano-Nelson model lie on an ellipse centered to the

origin [Fig. 3.2(a)]. Using Bloch's theorem, we may in fact extract an exact expression for the eigenvalues in the limit $N \to \infty$ in terms of the wavenumber k:

$$\omega(k) = 2\cosh(h)\cos(k) - 2i\sinh(h)\sin(k) \tag{3.8}$$

for $k \in [0, 2\pi]$. The sign of h determines the direction of the elliptical contour described in the complex plane when varying k monotonically. This quantity is more commonly defined in terms of the winding number w as:

$$w = \int_0^{2\pi} \frac{dk}{2\pi} \frac{d\omega(k)}{dk} \tag{3.9}$$

For the PBC Hatano-Nelson model of Eq. (3.1), w takes the values $w = \pm 1 = -\text{sgn}(h)$ which correspond to counterclockwise and clockwise trajectories in the complex plane [65].

Because asymmetric transport is not limited by the size of the system as in the case of the OBC Hatano-Nelson lattice, an excitation on any site of the lattice can be amplified as it asymmetrically transports in the preferred direction of the lattice; the wave that transports in the opposite direction likewise decays exponentially and eventually vanishes. At large propagation distances the most gainy modes will have dominated and eventually the field $|\psi(z)\rangle$ is amplified at a steady rate $4|\sinh(h)|$ [Figs. 3.2(b) and Figs. 3.2(c)].

Neither the OBC nor the PCB case of the periodic Hatano-Nelson model exhibits jumps in their dynamics; in the case of OBC, the evolution of the field exhibits oscillatory behavior, while in the case of PBC, we observe that the normalized field propagates asymmetrically in one direction, indicating that the non-normalized field is amplified. This reinforces the hypothesis that jumps are expected to take place only between localized states. To observe jumps in the Hatano-Nelson model, we need to introduce disorder to the system.

3.2 The Hatano-Nelson model with real disorder

The Hatano-Nelson model with real disorder is described, similarly to the Anderson model, by the Hamiltonian of Eq. (3.1) where the on-site potential ϵ_n is now drawn from the rectangular distribution of Eq. (2.3). After a brief summary of the effect of disorder on the spectrum and the eigenstates, we examine whether this system, which exhibits both non-Hermiticity and disorder, can exhibit jumps similar to those of the Anderson lattice for complex disorder (as seen in Fig. 2.7).

3.2.1 Localization of the eigenstates

We first remark that the non-Hermitian skin effect will dissipate for strong disorder, where the real diagonal dominates the off-diagonal asymmetric hopping amplitude terms. In this regime, we expect that all eigenstates will be localized and exhibit negligible gain or loss, as all eigenvalues will tend to the real axis.

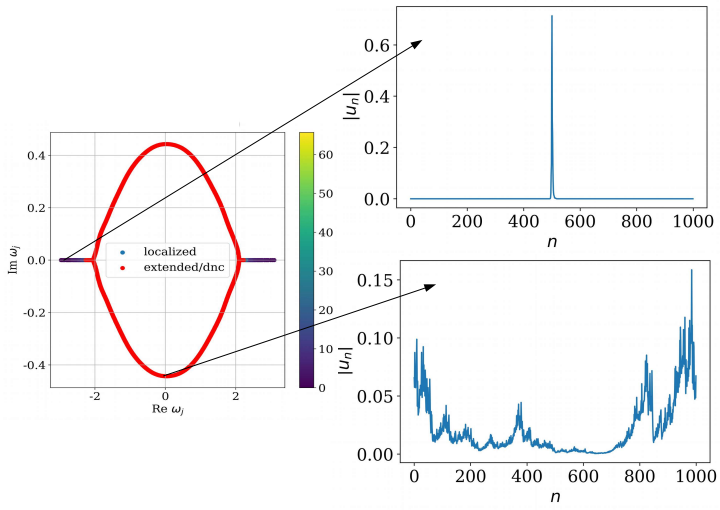

Figure 3.3: Procedural localization of the eigenstates of a lattice described by the Hatano-Nelson Hamiltonian of Eq. (3.1) under PBC and $h = 0.1$ with disorder strength $W = 2$, calculated using the transfer matrix method, with the spectrum plotted in the complex plane as in Fig. 2.1. The color map represents the localization length, while the red dots represent the part of the spectrum for which the states are characterized by a localization length $\xi \gtrsim N$ and the calculation does not converge. Two representative states are plotted; states with eigenvalues at the edge of the band are localized and have eigenvalues tending closely to the real axis, while eigenstates with eigenvalues near the center of the band (on the ring part of the spectrum) behave as extended ($\xi > N$). ($N = 1000$)

As a result, for strong enough disorder the boundary conditions will not be significant.

As in the case of the tight-binding Hamiltonian, we may calculate the localization length for each eigenvalue ω_j of the Hatano-Nelson model with a random on-site potential ϵ_n by using the transfer matrix method. In analogy to the derivation of Eq. (2.7) for the Anderson model, we derive the transfer matrix for the Hatano-Nelson Hamiltonian as:

$$\begin{bmatrix} \psi_{n+1} \\ \psi_n \end{bmatrix} = \begin{bmatrix} (\omega - \epsilon_n)e^h & -e^{2h} \\ 1 & 0 \end{bmatrix} \begin{bmatrix} \psi_n \\ \psi_{n-1} \end{bmatrix} \equiv \hat{T}_n \begin{bmatrix} \psi_n \\ \psi_{n-1} \end{bmatrix} \tag{3.10}$$

so that Eq. (2.7) applies as in the case of the Anderson lattice. We remark that we may also obtain an average value for the localization length in selected sections of the bands by fitting $\ln|\psi_n| - n$ as outlined in Sec. 2.1.1.

For the Hatano-Nelson model of Eq. (3.1) under PBC, we observe that strong localization of an eigenstate implies that its eigenvalue will have a negligible

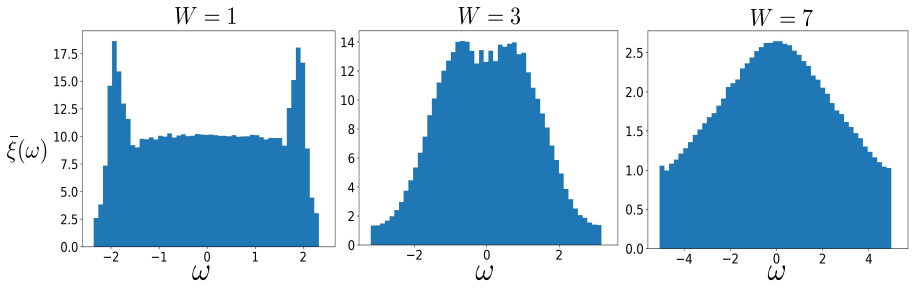

Figure 3.4: Average localization length $\bar{\xi}$ as a function of the eigenvalue ω for the right eigenstates $|u^R\rangle$ of the Hatano-Nelson model under OBC with $h = 0.1$ for different values of the real disorder strength $W = 1$, $W = 3$, $W = 7$, calculated as in Fig. 2.2. Note that for weak disorder the eigenstates around the center of the band (which are the least affected by disorder) are localized with $\xi \sim 10$ whereas they are extended ($\xi > N$) in the cases of the Hermitian Anderson model or the Hatano-Nelson model under PBC. For the case of $W = 1$, the localization length is larger for eigenstates with eigenvalues at the edges of the band, as the the effect of disorder is to deform edge states into states localized anywhere on the lattice. The transition between the bulk localized and the skin effect phases of the system is hence marked by an increase in the localization length of the edge states as they are deformed.

imaginary part [Fig. 3.3]. Without disorder, the eigenstates are all extended and their corresponding eigenvalues lie on the ellipse described by Eq. (3.8); as the real disorder increases, the eigenstates become increasingly localized and because the real diagonal term dominates the non-reciprocal coupling, their eigenvalues tend to the real axis. For strong enough disorder, the spectrum becomes real and the eigenstates exhibit negligible gain or loss.

In the case of the Hatano-Nelson model under OBC, the states are already localized as a result of the NHSE in one edge of the lattice even without the presence of disorder; by the discussion of the previous section, we expect that the localization length of the eigenstates will be $\xi \sim 1/|h|$. For strong disorder, the eigenstates are localized anywhere on the lattice in accordance with Anderson localization. This transition is mediated by a continuous deformation of the eigenstates and the spectrum; as a result, the localization length is expected to increase for weak disorder as the NHSE dissipates [Fig. 3.4].

We conclude that there are no localized modes that exhibit gain or loss in the case of real disorder, so the key assumption (strongly localized states that exhibit gain or loss) that was used in the case of the Anderson model with complex disorder to predict and explain the delocalization via jumps does not hold here; this is a strong indication that the Hatano-Nelson model does not exhibit jumps.

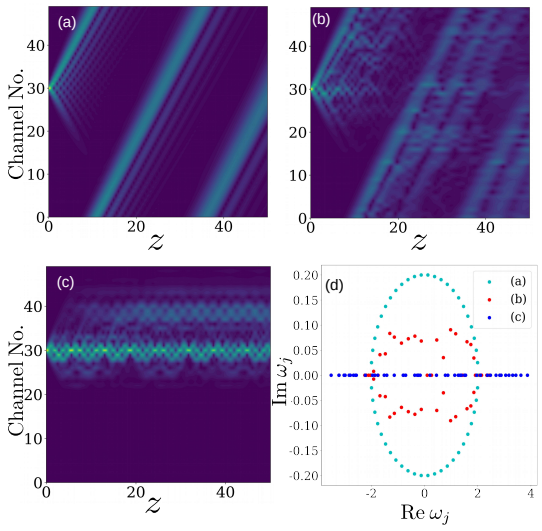

Figure 3.5: Propagation of a single-channel excitation for the same realization of the Hatano-Nelson Hamiltonian formulated in Eq. (3.1) with varying disorder strength, system size of $N = 50$, $h = 0.1$ and PBC. (a) No disorder. Every eigenstate is extended and the eigenvalues form a closed ring. (b) Weak real disorder $W_R = 2$. Some eigenstates with real eigenvalues are localized, while others are extended. (c) Strong real disorder $W_R = 6$. There are no extended eigenstates, and the initial excitation remains localized in the right section of the lattice. (d) Spectra for each of the above realizations (a-c).

3.2.2 No jumps in the Hatano-Nelson model

For the reasons outlined in the previous section, the dynamics of the Hatano-Nelson model does not feature jumps under any choice of boundary conditions.

Under OBC, the right eigenstates are all concentrated on one edge of the lattice; an initial excitation propagates asymmetrically to that side until it reaches the boundary. At that point, the optical power reaches its maximum value and then oscillates, as seen in Fig. 3.1. The frequency of the oscillation depends on the size of the lattice. The addition of real diagonal disorder localizes the eigenstates without affecting the reality of the spectrum; as a result, the field remains localized and no dynamical delocalization is exhibited.

Under PBC, the dynamics of an initial excitation are characterized by the domination of the most gainy eigenstate. Since the eigenstates are all extended, asymmetric transport is not inhibited and the optical power increases exponentially. Because the addition of real disorder localizes the eigenstates while simultaneously decreasing their amplification/dissipation rates, gain or loss cannot coexist with strong localization in such a lattice. As a result, no jumps are observed, as seen in Figs. 3.5(a-c).

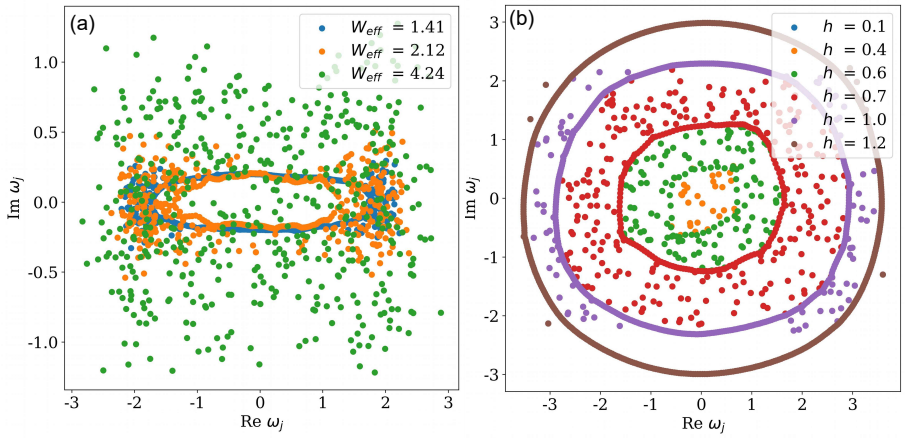

Figure 3.6: Phase transition between the mixed and the bulk localized phase exhibited in the spectrum of the PBC Hatano-Nelson Hamiltonian ($N = 500$) with complex disorder in the form of Eq. (2.15). (a) Spectrum for $h = 0.1$ and variable disorder strength with $W_R = W_I$. As the disorder strength increases, more states become localized and the ring deforms, until a critical disorder value is reached and all states become localized. (b) Spectrum for $W_R = W_I = 5$ and variable h. Localized states behave inflexibly and are not sensitive to the asymmetry of the hopping amplitudes once they become localized. For low values of h (between $h = 0.1$ and $h = 0.4$), the spectrum is entirely dominated by the complex diagonal potential.

The absence of jumps in the dynamics of the Hatano-Nelson model with real disorder indicates that non-Hermiticity and strong disorder is a necessary but not sufficient condition for delocalization via jumps.

3.3 A modified Hatano-Nelson model

In this section, we introduce complex on-site disorder to the Hatano-Nelson Hamiltonian of Eq.(3.1) in the form of the random distribution in Eqs.(2.15) and (2.25) (loss only). The spectrum of the Hatano-Nelson model in this case exhibits a phase transition in the complex plane which relates to whether its eigenstates are partially or fully localized. In the last case we recover the jumpy dynamics exhibited by the Anderson model with complex disorder as seen in Sec. 2.2.2. We also examine the case of off-diagonal Hermitian disorder; in this case, where the non-Hermiticity is provided only by the asymmetric terms in the Hatano-Nelson Hamiltonian, we also recover the jumps.

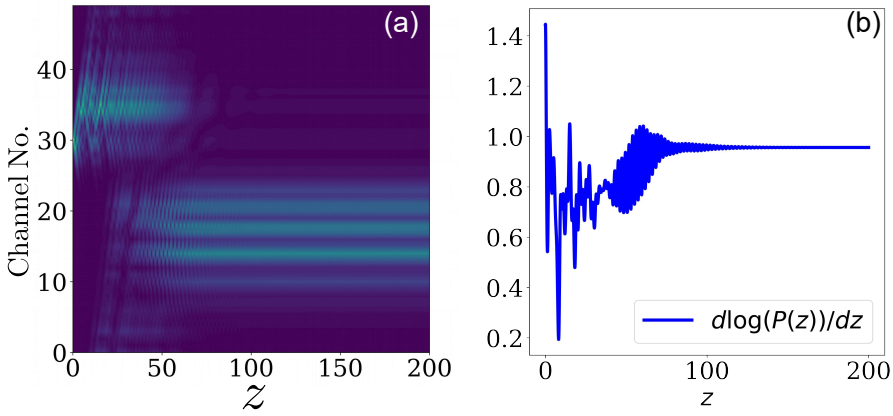

Figure 3.7: Spectrum and dynamics for a lattice described by Eqs. (3.1) under PBC and (2.15) with $N = 50$, $h = 0.1$, in the weak complex disorder regime ($W_R = W_I = 1.5$). (a) Evolution of the normalized field for a single-channel excitation on $n = 43$, which exhibits no clear jumps. (b) Derivative of the power logarithm. No jumps can be observed to take place. The field dissipates at an average rate determined by the on-site loss near the excitation channel.

3.3.1 The Hatano-Nelson model with complex disorder

We initially consider the Hatano-Nelson model of Eq.(3.1) under PBC with random complex on-site potential ϵ_n drawn from the even distribution of Eq. (2.15), as in the Anderson model with complex disorder. The effect of increasing the effective disorder strength W_{eff} is a continuous deformation of the spectrum from its elliptical shape in the case of no disorder, similar to the deformation shown in Fig. 3.3 for real diagonal disorder.

For given h, as the disorder strength increases, states starting on the edge of the band become localized, and the ring that consists of those states that remain extended shrinks. After a critical value of disorder, all states are localized and the elliptical shape that the spectrum exhibits in the non-disordered case vanishes entirely [Fig. 3.6(a)]. The system therefore exhibits two phase transitions; one between the delocalized phase where there are only complex extended states and the mixed phase where localized states begin to appear at the edge of the band, and one between the mixed phase and the bulk localized phase which is characterized by the complete absence of extended states [68]. The phase that the spectrum appears in is determined by the ratio of the effective disorder $W_{\text{eff}} = \sqrt{W_R^2 + W_I^2}$ and the hopping amplitude $e^{|h|}$. The deformation of the spectrum and the associated localization length is examined in greater detail in Fig.B.1 under OBC.

We note that the spectrum of the PCB Hatano-Nelson model in the case of the bulk localized phase (Fig. 3.6a, green dots) appears almost identical to the

spectrum of the tight-binding Anderson model in the case of strong complex disorder (Fig. 2.5(b)), and so it may exhibit jumps as well. In the case there are many localized states that are more gainy than the extended states in the mixed phase, it may also be possible to observe jumps between those states, if these eigenstates are also strongly localized. In the next sections, we will explore these two possibilities.

3.3.2 Jumps in the complex Hatano-Nelson model

We initially comment that the case of weak complex disorder, which corresponds to the spectrum being in the mixed phase seen in Fig. 3.6(a) (orange dots), does exhibit some of the characteristics of delocalization via jumps, but because of an abundance of extended states, jumpy propagation cannot be distinguished from gainy transport as the field transports asymmetrically to one direction of the lattice (Fig. 3.7).

We now consider the Hatano-Nelson model with strong complex diagonal disorder in the form of a rectangular distribution with only loss per Eq.(2.25). The spectrum is in the bulk localized phase as in Fig. 3.6(a) (green dots), but is confined in the lower complex plane, indicating that the effect of gainy transport that appeared in the case of the periodic Hatano-Nelson model has completely diminished and the asymmetry of the two coupling constants in Hamiltonian of Eq. (3.1) has been dominated by the diagonal terms. Furthermore, the strong disorder causes the NHSE to be supressed (as in the Hermitian case) and the choice of boundary conditions does not affect the spectrum and the dynamics of the system. The dynamics of this model feature clear jumps as in the case of the Anderson model with complex disorder, seen in Fig. 3.8a. Since jumps appear from the right to the left side of the lattice, we conclude that propagation is not chiefly affected by the asymmetry of the coupling constants which favors propagation to the right in this case ($h > 0$).

We also note that oscillatory behavior is exhibited in the jump between states 44 and 47 as evidenced in Figs. 3.8(a) and 3.8(c) in both the normalized field dynamics and the derivative of the logarithm optical power. Because these states are localized at neighboring lattice sites and the magnitudes of their projection coefficients in similar in a propagation interval, while the imaginary parts of their eigenvalues are comparable [Fig. 3.8(d)], the almost-orthogonal approximation of Eq. (2.29) does not hold well for these states, and their non-orthogonality is responsible for the observed power oscillation. By calculating the optical power from Eq. (2.28) including only the terms related to the dominant eigenstates as determined by Fig. 3.8(b) as well as the corresponding overlaps in the $\Gamma_{i,j}$ matrix, we recover this oscillation [black dashed line in Fig. 3.8(c)].

3.3.3 The Hatano-Nelson model with Hermitian off-diagonal disorder

Motivated by the above results, we look for another modification to the Hatano-Nelson model. We may also consider, in addition to a real diagonal disorder

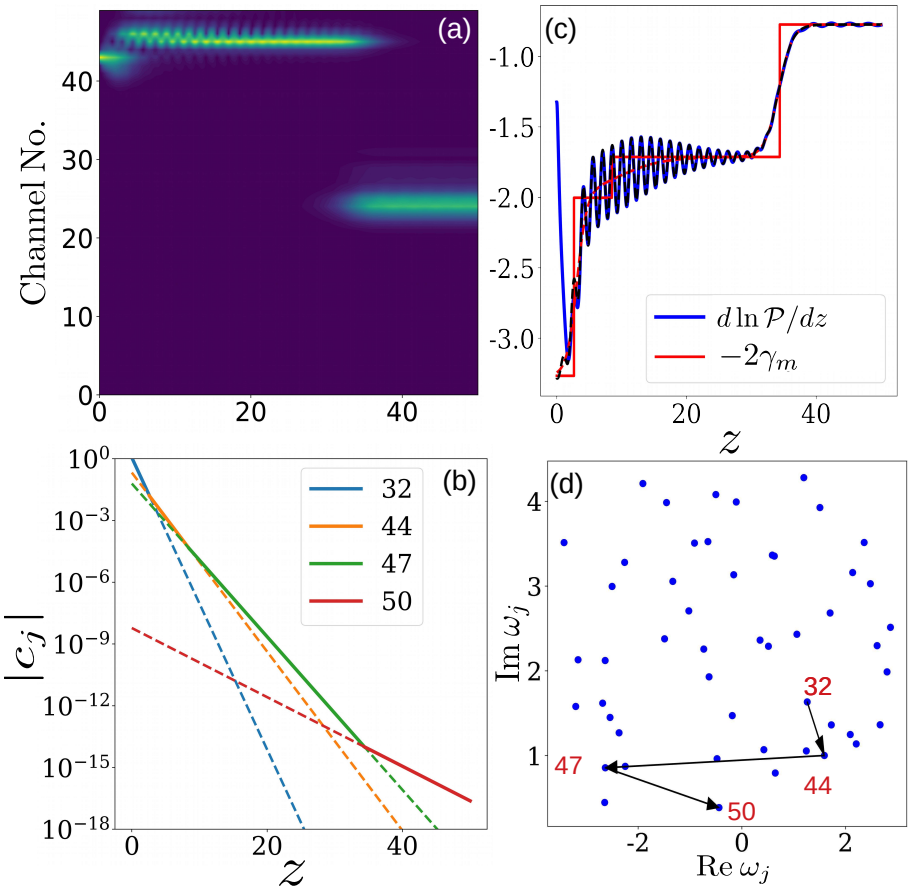

Figure 3.8: Jumpy evolution of the Hatano-Nelson mode of Eq. (3.1) under OBC with $N = 50$, in the strong complex disorder regime ($W_R = W_I = 5$, $h = 0.1$) with only loss per Eq. (2.25). (a) Evolution of the normalized field amplitude $|\psi_n|$ for a single-channel excitation on channel $n = 43$, with one distinctive jump. (b) Magnitude of the projection coefficients, as in Fig. 2.9(b). (c) Derivative of the power logarithm, as in Fig. 2.9(a). Note the oscillatory behavior present in the first jump. The black dashed line gives the expected evolution of the optical power given by Eq. (2.28) including only dominant modes without the orthogonality approximation. d) Spectrum, with all eigenvalues corresponding to lossy localized states. The most distinctive jump is between modes 47 and 50. The most distinctive jump is between modes 47 and 50.

term, a Hermitian off-diagonal disorder term to the Hatano-Nelson Hamiltonian ([72] - [73]) as:

$$\hat{H} = \sum_{n=1}^{N} \left[\epsilon_n |n\rangle \langle n| + (e^{-h} + v_n) |n+1\rangle \langle n| + (e^{h} + v_{n-1}^{*}) |n\rangle \langle n-1| \right] \quad (3.11)$$

where ϵ_n is a real disorder term drawn from a rectangular distribution as in Eq. (2.3), and v_n are the matrix elements of the off-diagonal Hermitian disorder term in the Hamiltonian. Equivalently, we can write the equations for the evolution of the field on each channel as:

$$i\frac{\partial \psi_n}{\partial z} + (e^{h} + v_{n-1}^{*})\psi_{n-1} + (e^{-h} + v_n)\psi_{n+1} \quad (3.12)$$

We may define the disorder strength for the off-diagonal disorder by taking $v_n \equiv |v_n| e^{i\beta_n}$ where $|v_n|$ and β_n are drawn from the random distribution describing a disk of radius V in the complex plane:

$$|v_n| \in [0, V],\ \beta_n \in [0, 2\pi] \quad (3.13)$$

This implementation of off-diagonal disorder in the Hatano-Nelson model can be experimentally realized by modulating the amplitude and the phase of the field as it exits each waveguide, instead of introducing gain or loss locally is in the case of complex diagonal disorder. Because the off-diagonal disorder is taken to be Hermitian, the only source of non-Hermiticity in this Hamiltonian is the inherent asymmetry of the coupling constants in the Hatano-Nelson model.

We initially take $\epsilon_n = \epsilon = 0 \forall n$, such that the Hamiltonian describes a periodic Hatano-Nelson model with additional Hermitian off-diagonal terms. Because of the periodic on-site potential, the spectrum is symmetric about the origin of the complex plane. The effect of increasing off-diagonal disorder on the spectrum continuously shrink the region of the band inside of which extended states lie, similarly to the case of complex diagonal disorder [Fig. 3.9(a)]. An important distinction to be made for this case versus the case of only diagonal real disorder is that the imaginary gauge transformation that forces a real spectrum for the Hatano-Nelson model under OBC and reduces it to a tight-binding model with reciprocal couplings no longer applies, and as result the spectrum is in general complex even in this case [Fig. 3.9(b)]. We therefore may have a complex spectrum without relying on on-site pumping or dissipation via leaks on each waveguide site.

The effect of the disorder on the eigenstates is similarly a continuous deformation. An interesting feature of off-diagonal disorder is that, unless an exponential random distribution is chosen for $|v_n|$, there are some extended states near the center of the band regardless of the disorder strength; this occurs because in the case of a large value of V there are some large transfer matrix elements between the sites and thus transport is favored over localization [74]. This effect is shown for the continuous deformation of an eigenstate for the case of the model under OBC in Fig. B.2. Therefore, the use of off-diagonal disorder enables us to also study the effect of the presence of extended states in the spectrum.

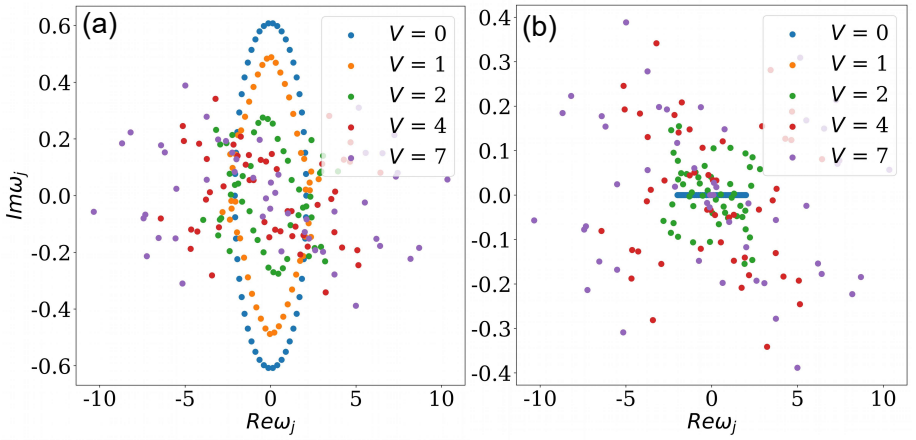

Figure 3.9: Deformation of the spectrum of the Hatano-Nelson model with the addition of off-diagonal disorder described by Eqs. (3.11) and (3.13), with $h = 0.3$, $N = 50$, no diagonal disorder ($W = 0$) and variable off-diagonal disorder strength V. (a) Deformation of the spectrum for periodic boundary conditions. The states near the center remain extended and fluctuate significantly as V increases. (b) Deformation of the spectrum for closed boundary conditions. Note that the spectrum is no longer real, but is generally complex because the asymmetry of the coupling constants can no longer be lifted by introducing a local gauge transformation, is in the periodic case.

Because of the existence of strongly localized states that correspond to eigenvalues in the edge of the band in complex plane, the almost orthogonal approximation of Eq. (2.29) that is necessary for the application of Eqs. (2.30) and (2.31) is valid at least concerning these states. For this reason, we expect that such a model will also exhibit jumps, in spite of the Hermitian disorder. The propagation of a single channel excitation in a lattice described by the Hamiltonian of Eq. (3.11) does indeed show that this occurs, as seen in Figs. 3.10(a-c).

We comment that the addition of real diagonal disorder as per Eq. (2.3) to the Hermitian disorder term will result in a decrease for the localization length of the eigenstates and the collapse of the spectrum to the real axis if $W \gg V$. For small values of the diagonal disorder strength W we still expect the spectrum to be complex and therefore jumps will take place, albeit over larger propagation distances as the absolute imaginary parts of the eigenvalues will be decreased.

3.4 Summary and Discussion

The Hatano-Nelson model introduces non-Hermiticity by replacing the coupling term between two sites in the tight-binding Hamiltonian with two asymmetric

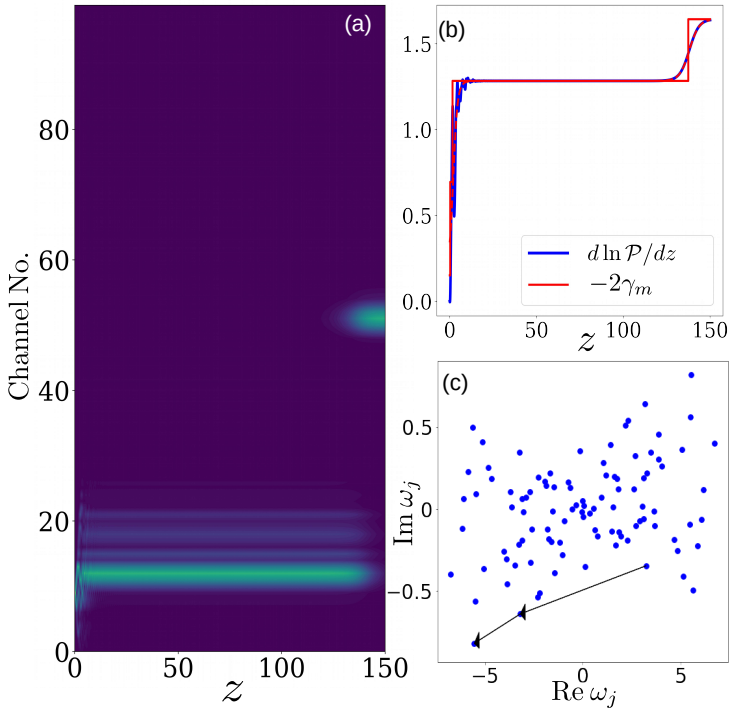

Figure 3.10: Dynamics of the normalized field and spectrum for a system described by the Hatano-Nelson model with off-diagonal disorder of Eqs. (3.11) (under PBC) and (3.13) with $h = 0.5$, $N = 50$ and $V = 5$, $W = 0$ (no diagonal disorder). (a) Evolution of the normalized field amplitude $|\phi_n|$ for a single channel excitation on $n = 9$ with one, distinct jump. (b) Derivative of the power logarithm for the dynamics in (a), as in Fig. 2.9(a). (c) Spectrum in the complex and eigenvalues of the dominant modes participating in the jump seen in Fig. 2.8(c).

coupling constants [Eq. (3.1)], therefore inducing a preferred direction in which the field is amplified as it is transported [Fig. 3.2]. The choice of boundary conditions for the system greatly influences its spectral and dynamical properties, causing the localization of the eigenstates to one edge of the lattice as seen in Sec. 3.1; this phenomenon is known as the NHSE. The addition of real disorder causes the eigenstates to become localized while reducing the absolute imaginary parts of their respective eigenvalues, while supressing the NHSE. For the case of PBC, only extended eigenstates correspond to complex eigenvalues, while for the case of OBC the spectrum remains real at all times. Therefore, it does not exhibit delocalization via jumps [Figs. 3.5(a-b)]. The introduction of complex disorder per Eqs. (2.15) or (2.25) (loss only) in the Hatano-Nelson Hamiltonian causes the appearance of 3 distinct phases in the Hatano-Nelson spectrum [Figs.

3.6(a-b)]; when the spectrum is in the bulk localized phase for strong complex disorder, the diagonal disorder term dominates and jumps can be observed as in the tight-binding Anderson model with complex disorder [Figs. 3.8(a-c)]. Another case which exhibits jumps without introducing gain or loss locally is that of the Hatano-Nelson model with additional off-diagonal disorder per Eq. (3.11), which also displays delocalization via jumps between strongly localized gainy eigenstates (Fig. 3.10).

From the results of this section, we can infer that a non-Hermitian system will not necessarily exhibit delocalization via jumps if it has localized eigenstates; the additional requirement is that the eigenvalues associated with these eigenstates must also be complex.

Chapter 4

Conclusions

The results in this work indicate that a form of dynamical delocalization, namely delocalization via jumps, can be observed when introducing non-Hermiticity to disordered lattices. This type of propagation occurs between localized eigenstates that exhibit gain or loss, observed in the dynamics of the normalized field amplitude $|\phi(z)\rangle$ as a sudden "jump" of the field between distant sites of the lattice as well as the derivative of the power logarithm, which is an experimentally measurable quantity. This dynamical evolution is adequately captured by the analytical approximate forms for the optical power in Eqs. (2.30) and (2.31). Based on the case studies of both the symmetrical non-Hermitian Anderson model and the asymmetric Hatano-Nelson model, delocalization via jumps is expected to be observed in all cases where the system is described by a complex spectrum with localized eigenstates, regardless of the disorder strength, such that the almost orthogonal approximation of Eq. (2.29) applies to the right eigenstates. The effect of weak disorder is then to obfuscate the jumps by introducing some extended states to the spectrum.

Because jumps can also be observed in the case of only loss, delocalization via jumps is not an effect that results from selective amplification of the field on specific sites via the addition of external energy. In the Hermitian case, energy is transported through the evanescent coupling of adjacent channels in the lattice; this mechanism is blocked in the presence of strong disorder via Anderson localization. The effect of non-Hermitian disorder is to introduce complex eigenvalues which enable the propagation of energy via jumps, and thus overcome Anderson localization. If the disorder is strong enough, alternative propagation mechanisms are eliminated and thus the observation of jumps is facilitated.

As a general conclusion, delocalization via jumps is an observable effect that arises from the interplay of non-Hermiticity and strong disorder in photonic lattices. Our results indicate that non-Hermiticity provides new and interesting alternatives to Anderson localization in the case of disordered systems and exploits the meaning of wave transport.

Appendix A

Jumps in 2-D lattices

In this chapter we will examine delocalization via jumps in 2-D tight-binding lattices, starting from the Anderson model in two dimensions and continuing with a non-reciprocal non-Hermitian model consisting of coupled Hatano-Nelson chains. Since we have established the conditions under which delocalization via jumps is expected to take place, we will initially examine whether almost orthogonal approximation of Eq. (2.29) for the right eigenstates is valid by examining their localization length and orthogonality matrix. Afterward we will examine the second order NHSE exhibited in the case of the non-reciprocal lattice. In both cases, jumps are exhibited under similar conditions to the one-dimensional cases.

A.1 The 2-D tight-binding Anderson model

In this section we examine the 2-D tight binding Anderson model by considering a rectangular lattice of size $M \times N$ with random complex on-site potential drawn from a rectangular distribution as in Eq. (2.15) or Eq. (2.25) (loss only). The Hamiltonian that describes this lattice is given by:

$$\hat{H} = \sum_{m=1,n=1}^{M,N} \epsilon_{m,n} \left|m,n\right\rangle \left\langle m,n\right| + c \sum_{m,m',n,n'}{}' \left|m,n\right\rangle \left\langle m',n'\right| \tag{A.1}$$

where the accented sum denotes summation over nearest neighboring lattice sites (either $|m-m'|=1$ or $|n-n'|=1$). As with the rest of this work, we take $c=1$. For the boundary conditions, we may choose independently periodic or open boundary conditions for each of the two directions. We denote these

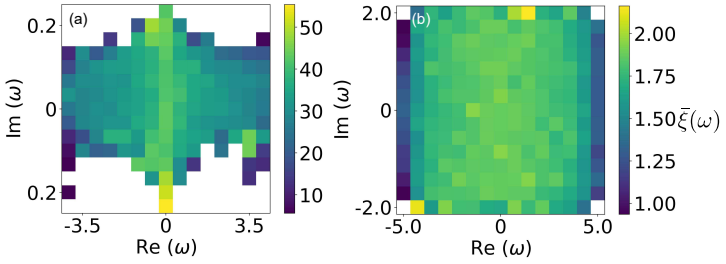

Figure A.1: Spectrum and average localization length $\bar{\xi}(\omega)$ (colorbar) as a function of the complex eigenvalues ω for the 2-D tight binding Anderson model of Eq. (A.1) with complex disorder in the form of Eq. (2.15), averaged for 50 realizations for a lattice size of 40×40. (a) Weak complex disorder with $W_R = W_I = 1$. The localization length is comparable to the system size. (b) Strong complex disorder with $W_R = W_I = 5$. In this regime we expect that the right eigenstates are almost orthogonal.

choices as:

$$\begin{aligned}
&\text{OBC}: |0,n\rangle = |m,0\rangle = |M+1,n\rangle = |m,N+1\rangle = 0 \\
&\text{PBC}_x: |0,n\rangle = |M+1,n\rangle = 0,\ |m,N+1\rangle = |m,1\rangle\,,\ |m,0\rangle = |m,N\rangle \\
&\text{PBC}_y: |m,0\rangle = |m,N+1\rangle = 0\ |M+1,n\rangle = |1,n\rangle\,,\ |0,n\rangle = |M,n\rangle \\
&\text{PBC}_{xy}: |m,N+1\rangle = |m,1\rangle\,,\ |m,0\rangle = |m,N\rangle\,,\ |M+1,n\rangle = |1,n\rangle\,,\ |0,n\rangle = |M,n\rangle
\end{aligned} \tag{A.2}$$

In the cases of mixed boundary conditions PBC_x and PBC_y, the system is described by the topology of an open cylinder, while in the case PBC_{xy} (toroidal boundary conditions) the system is described by the topology of a torus. We note that since our model consists of stacked chains that do not mix the two directions, in the case of no disorder its $M \times N$ eigenvalues will be of the form:

$$\omega = \omega_{i,j} = \omega_i^M + \omega_j^N \tag{A.3}$$

where ω^M and ω^N denote the eigenvalues for the 1-D tight binding Anderson model of Eq. (2.4) under the boundary conditions applied in each direction for system sizes M and N respectively and i, j are integer indices such that $i \in [1, M]$ and $j \in [1, N]$.

A key difference between the 1-D and the 2-D case for the Anderson model that has been developed upon in the context of the scaling theory of localization is that for an infinite two-dimensional system, while all states are localized as in the one-dimensional model, the localization length scales exponentially with the mean free path of the wave as it is scattered by the on-site impurities. For a finite lattice, we expect this to translate in practice to the necessity of a higher disorder strength to observe strong localization for the eigenstates of the lattice, and therefore obtain the jumps associated with their orthogonality.

To calculate the localization length, we employ the linear fit to the logarithm of the eigenstate magnitudes outlined in Sec. 2.1.1 and in particular Eq. (2.9). To adapt this method to a second spatial dimension we fit independently for both the x and y direction of the lattice and then average the results according to the size of the lattice in both directions:

$$\bar{\xi}_j = \frac{N\xi_{jx} + M\xi_{jy}}{M+N} \tag{A.4}$$

where M is the number of rows, N is the number of columns, and ξ_{xy} is the localization length obtained for averaging along the x/y direction. The reasoning for such an averaging is that the coupling constant for each tight-binding chain in the model is the same in both the x and y directions. In general, the localization length may be different for each direction. We then bin the eigenvalues ω_j in rectangular regions of equal area in the complex plane and average the localization length in each region to obtain an estimate for $\bar{\xi}(\omega)$. The results of this analysis are shown in Figs. A.1(a-b). These results indicate that in the strong disorder regime the eigenstates decay exponentially outside a region limited to few lattice sites, and therefore we expect that the almost orthogonal approximation of Eq. (2.29) will also hold here.

We remark that our derivations for the approximate form of the derivative of the logarithm power of Eqs. (2.30) and (2.31) are based on the biorthogonality condition of Eq. (2.16), and therefore also apply to the case of two-dimensional lattices with on-site disorder. To calculate the field dynamics, we use the exponential matrix method of Eq. (2.14). Our results using the same methodology formulated for one-dimensional lattices in Sec. 2.2.2 are summarized in Figs. A.2(a-d). Note that because all the eigenstates as well as the initial excitation are localized and there is a higher number of neighboring sites for the initial excitation due to the two-dimensional structure of the lattice there are more modes with high initial values of their respective projection coefficient magnitudes [Fig. A.2(b)], resulting in more modes participating in jumpy propagation as well as a more complex evolution of the derivative of the power logarithm [Fig. A.2(c)].

A.2 Rectangular 2-D non-reciprocal lattice

For this section we consider a 2-D non-reciprocal tight binding lattice consisting of stacked Hatano-Nelson chains [Eq. (3.1)] ([70]). The Hamiltonian describing this model can be written as:

$$\begin{aligned}\hat{H} = &\sum_{m=1,n=1}^{M,N} \epsilon_{m,n} \left|m,n\right\rangle \left\langle m,n\right| \\ &+ \sum_{m=1,n=1}^{M,N} \left[e^{-h_x} \left|m,n\right\rangle \left\langle m,n+1\right| + e^{h_x} \left|m,n\right\rangle \left\langle m,n-1\right|\right] \\ &+ \sum_{m=1,n=1}^{M,N} \left[e^{-h_y} \left|m,n\right\rangle \left\langle m+1,n\right| + e^{h_y} \left|m,n\right\rangle \left\langle m-1,n\right|\right]\end{aligned} \tag{A.5}$$

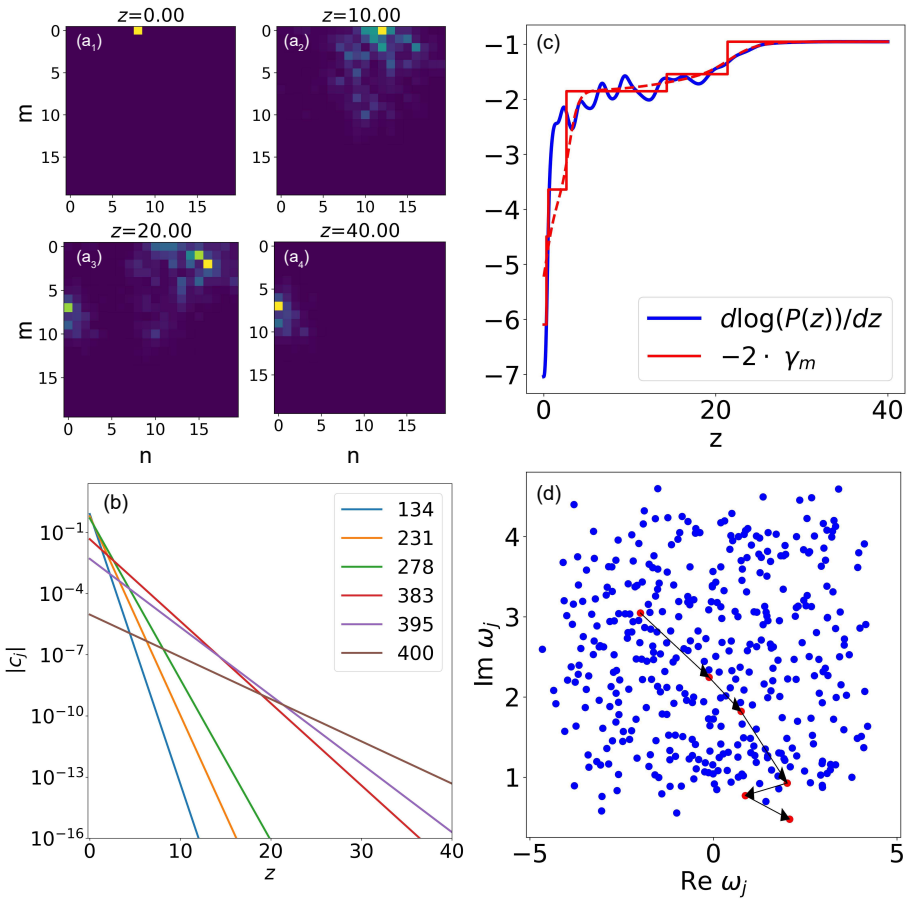

Figure A.2: Jumpy evolution of the normalized field $|\phi\rangle$ for the two-dimensional complex Anderson model described by Eqs. (A.1) and (2.25) (loss only) under OBC with $W_R = W_I = 5$ for a lattice of size 20×20. (a_1 - a_4) Two-dimensional normalized field profile for the initial excitation at $(m, n) = (1, 9)$ and its evolution at $z = 10$, $z = 20$ and $z = 40$. (b) Magnitudes of the projection coefficients for the dominant modes as in Fig. 2.9(b). (c) Derivative of the logarithmic power as in Fig. 2.9(a). (d) Spectrum and eigenvalues of the dominant modes which participate in the jumpy dynamics, as in Fig. 2.8(c). The eigenvalues of the dominant eigenstates are highlighted in red for clarity.

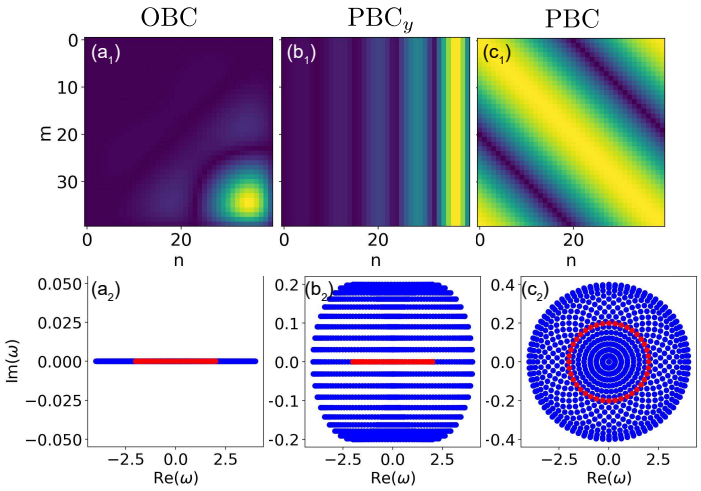

Figure A.3: Representative eigenstates (a_1, b_1, c_1) and spectra (a_2, b_2, c_2, blue dots) of the non-reciprocal 2-D lattice of Eq. (A.5) under OBC, PBC_y and PBC respectively, with $h_x = h_y = 0.1$ and $M = N = 40$. The red dots in (a_2),(b_2) and (c_2) represent the spectrum of the Hatano-Nelson model with system size N and $h = 0.1$ under the same boundary conditions as those applied in the x direction in each case.

where h_x and h_y determine the non-reciprocal coupling terms for the x and the y direction respectively, and the boundary conditions are considered as in Eqs. (A.2).

In the case that $h_x = 0$ and $h_y = 0$, we recover the tight binding Anderson model of Eq. (A.1). For only one nonzero h_x or h_y, the model displays a preferred direction of propagation for only one of the two axes x, y respectively. If both h_x and h_y are nonzero, both axes have a favored propagation direction and the system displays a second order non-Hermitian skin effect under OBC where the right eigenstates are localized in one corner of the lattice. Under PBC_x or PBC_y, the system displays the first order non-Hermitian skin effect where the states decay exponentially away from one of the edges of the lattice, depending on the choice of the direction in which the lattice is periodic.

As in the case of the Hatano-Nelson model, there is an imaginary gauge transformation of the form $\tilde{\psi}_{m,n} = \exp(-h_x n - h_y m)\psi_{m,n}$ which reduces the Hamiltonian of Eq. (A.5) to the 2-D tight binding Anderson model of Eq. (A.1). More generally, under PBC_x or PBC_y the Hamiltonian of this model can be rewritten to have reciprocal couplings in the y and x directions by a new choice of basis in the form $\tilde{\psi}_{m,n} = \exp(-h_y m)\psi_{m,n}$ or $\tilde{\psi}_{m,n} = \exp(-h_x n)\psi_{m,n}$ respectively. Under these considerations the right eigenstates will be localized in the directions where OBC are applied with localization lengths $1/|h_x|$ and $1/|h_y|$ for the x and y directions respectively.

The spectrum of this two-dimensional non-reciprocal model has the same form as in Eq. (A.3). As a result, we obtain wide landscape of spectra and eigenstates based on the order of the NHSE exhibited depending on the choice of the boundary conditions. A summary can be seen in Figs. A.3(a-c).

With the addition of complex diagonal disorder in the form of the distribution of Eq. (2.15), the spectrum deforms similarly as in the case of the Hatano-Nelson model. There are two distinctions to be made however. Firstly, for $h_x \neq h_y$ it is possible that the eigenstates will be more localized in one direction than the other because the stronger coupling. In this case, the average localization length may vary significantly when calculated along different directions for weak disorder strength. Secondly, the second order NHSE exhibited in the case of OBC is expected to more strongly localize the states in the corner of the lattice than the first order NHSE in the Hatano-Nelson model under OBC, and therefore stronger disorder is required to observe complete localization in the system.

As in the case of the Hatano-Nelson model, this model can also exhibit delocalization via jumps when it is in the bulk localized phase characterized by strong enough disorder to completely break the topology of the spectrum and localize the eigenstates. Our results are shown for a system in this regime in Figs. A.4(a-d) featuring one distinct jump at $z \sim 38$.

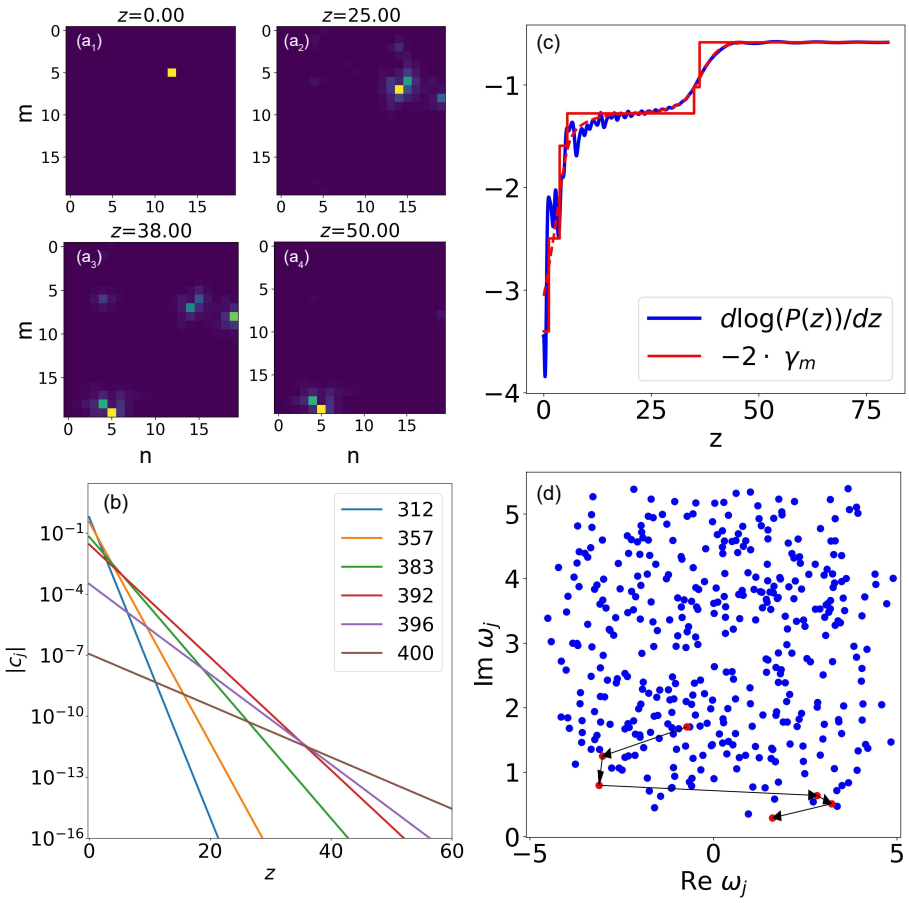

Figure A.4: Jumpy evolution of the normalized field $|\phi\rangle$ for the two-dimensional non-reciprocal model described by Eqs. (A.5) and (2.25) (loss only) under OBC with $W_R = W_I = 6$ for a lattice of size 20×20. (a_1 - a_4) Two-dimensional normalized field profile for the initial excitation at $(m, n) = (5, 11)$ and its evolution at $z = 25$, $z = 28$ and $z = 50$. (b) Magnitudes of the projection coefficients for the dominant modes as in Fig. 2.9(b). (c) Derivative of the logarithmic power as in Fig. 2.9(a). (d) Spectrum and eigenvalues of the dominant modes which participate in the jumpy dynamics, as in Fig. 2.8(c). The eigenvalues of the dominant eigenstates are highlighted in red for clarity.

Appendix B

Additional calculations

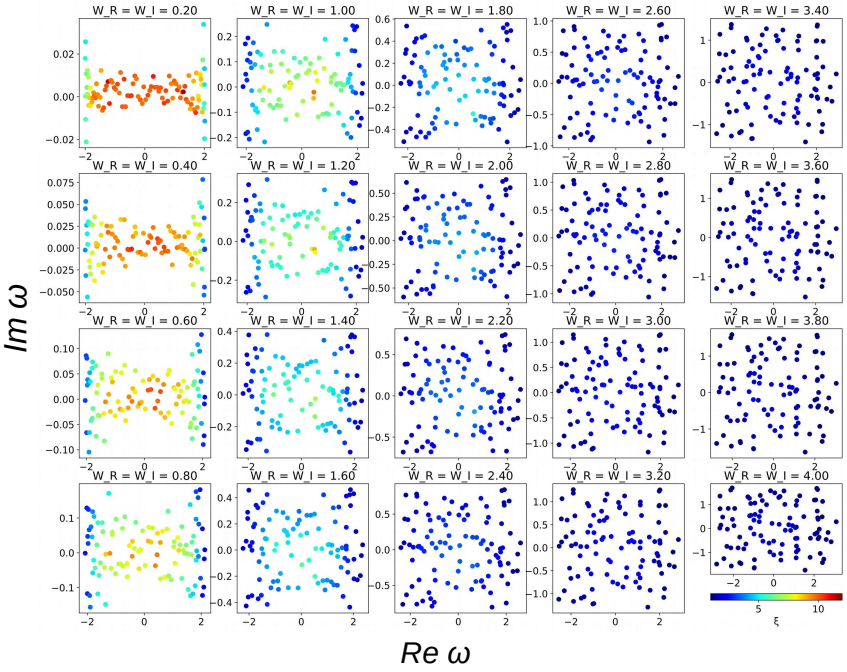

Figure B.1: Spectrum in the complex plane and localization length (color bar) for the Hatano-Nelson model of Eq. (3.1) under OBC with $h = 0.1$ and system size $N = 50$ for variable complex disorder in the form of Eq. (2.15), calculated using the transfer matrix method for a single realization of disorder.

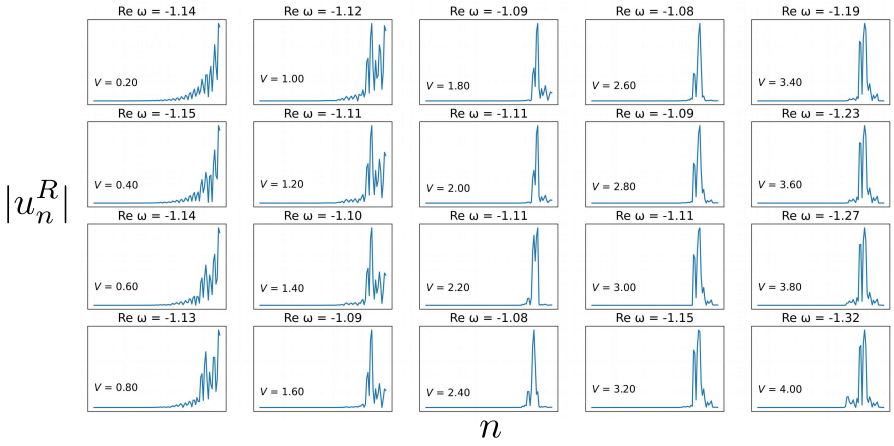

Figure B.2: Deformation of a single right eigenstate near the center of the band for the Hatano-Nelson model with Hermitian off-diagonal disorder described by Eq. (3.11) with $N = 50$, $h = 0.1$, $W = 0$ and variable V (denoted in each subfigure) under OBC. The real part of the eigenvalue of this eigenstate is denoted above each subfigure. Note that as V increases above a certain threshold the extend of the eigenstate also increases, corresponding to an increase in localization length.

Bibliography

[1] P. W. Anderson, Phys. Rev. **109**, 1492 (1958).

[2] E. Akkermans and G. Montambaux, *Mesoscopic Physics of Electrons and Photons* (Cambridge University Press, 2007).

[3] I. M. Lifshitz, S. A. Gredeskul, and L. A. Pastur, Introduction to the theory of disordered systems (Wiley Interscience, 1988).

[4] N. F. Mott and E. A. Davis, Electronic processes in non-crystalline materials (Oxford university press, 2012).

[5] P. W. Anderson, Philos. Mag. B, **52**, 505-509 (1985).

[6] E. Abrahams, P. W. Anderson, D. C. Licciardello, and T. V. Ramakrishnan, Phys. Rev. Lett. **42**, 673 (1979).

[7] A. Pal and D. A. Huse, Phys. Rev. B **82**, (2010).

[8] E. P. Wigner, Math. Proc. Camb. Phil. Soc. **47**, 790 (1951).

[9] R. A. Römer and M. Schreiber, *Numerical Investigations of Scaling at the Anderson Transition*, *Anderson Localization and Its Ramifications*, Lecture Notes in Physics **630** (Springer 2003).

[10] A. MacKinnon, *Numerical Investigations of Scaling at the Anderson Transition*, *Anderson Localization and Its Ramifications*, Lecture Notes in Physics **630** (Springer 2003).

[11] P. Markos and C. M. Soukoulis, *Wave Propagation* (Princeton University Press, 2008)

[12] E.N. Economou, *The Physics of Solids*, (Springer, 2010).

[13] D. N. Christodoulides, F. Lederer, and Y. Silberberg, Nature **424**, 817 (2003).

[14] D. S. Wiersma, P. Bartolini, A. Lagendijk and R. Righini, Nature, **390**, 671-673 (1997).

[15] D. S. Wiersma, Nature Photon 7, 188 (2013).

[16] A. Lagendijk, B. Van Tiggelen, and D. S. Wiersma, Phys.Today, **62**, 24 (2009).

[17] T. Schwartz, G. Bartal, S. Fishman, and M. Segev, Nature **446**, 52 (2007).

[18] Y. Lahini, A. Avidan, F. Pozzi, M. Sorel, R. Morandotti, D. N. Christodoulides, and Y. Silberberg, Phys. Rev. Lett. **100**, 013906 (2008).

[19] C. M. Bender and S. Boettcher, Phys. Rev. Lett. **80**, 5243 (1998).

[20] C. M. Bender, D. C. Brody, and H. F. Jones, Phys. Rev. Lett. **89**, 270401 (2002).

[21] C. M. Bender, Rep. Prog. Phys. **70**, 947 (2007).

[22] R. El-Ganainy, K. G. Makris, D. N. Christodoulides, and Z. H. Musslimani, Opt. Lett. **32**, 2632 (2007).

[23] K. G. Makris, R. El-Ganainy, D. N. Christodoulides, and Z. H. Musslimani, Phys. Rev. Lett. **100**, 103904 (2008).

[24] Z. H. Musslimani, K. G. Makris, R. El-Ganainy, D. N. Christodoulides, Phys. Rev. Lett. **100**, 030402 (2008).

[25] K. G. Makris, R. El-Ganainy, D. N. Christodoulides, and Z. H. Musslimani, Phys. Rev. A **81**, 063807 (2010).

[26] A. Guo, G. J. Salamo, D. Duchesne, R. Morandotti, M. Volatier-Ravat, V. Aimez, G. A. Siviloglou, and D. N. Christodoulides, Phys. Rev. Lett. **103**, 093902 (2009).

[27] C. E. Rüter, K. G. Makris, R. El-Ganainy, D. N. Christodoulides, M. Segev, and D. Kip, Nat. Phys. **6**, 192 (2010).

[28] O. Bendix, R. Fleischmann, T. Kottos, and B. Shapiro, Phys. Rev. Lett. **103**,030402 (2009).

[29] H. Ramezani, T. Kottos, R. El-Ganainy, and D. N. Christodoulides, Phys Rev. A **82**, 043803 (2010).

[30] M. C. Zheng, D. N. Christodoulides, R. Fleischmann, and T. Kottos, Phys. Rev. A **82**, 010103(R) (2010).

[31] Y. D. Chong, L. Ge, and A. D. Stone, Phys. Rev. Lett. **106**, 093902 (2011).

[32] L. Ge, Y. D. Chong, and A. D. Stone, Phys. Rev. A **85**, 023802 (2012).

[33] J. D. H. Rivero, M. Pan, K. G. Makris, L. Feng, and L. Ge, Phys. Rev. Lett. **126**, 163901 (2021).

[34] L. Ge and, A.D. Stone, Phys. Rev. X **4** 031011 (2014).

[35] N. Lazarides and G.P. Tsironis, Phys. Rev. Lett. **110**, 053901 (2013).

[36] G. Castaldi, S. Savoia, V. Galdi, A. Alu, and N. Engheta, Phys. Rev. Lett. **110**, 173901 (2013).

[37] A. Regensburger, C. Bersch, M.-A. Miri, G. Onishchukov, D. N. Christodoulides, and U. Peschel, Nature **488**, 167 (2012).

[38] L. Feng, Y.-L. Xu, W. S. Fegadolli, M.-H. Lu, J. E. B. Oliveira, V. R. Almeida, Y.-F. Chen, and A. Scherer, Nat. Mater. **12**, 108 (2013).

[39] B. Peng, S. K. Ozdemir, F. Lei, F. Monifi, M. Gianfreda, G. L. Long, S. Fan, F. Nori, C. M. Bender, and L. Yang, Nat. Phys. **10**, 394 (2014).

[40] L. Feng, Z. Jing Wong, R.-M. Ma, Y. Wang, and X. Zhang, Science **346**, 972 (2014).

[41] H. Hodaei, M.-A. Miri, M. Heinrich, D. N. Christodoulides, and M. Khajavikhan, Science **346**, 975 (2014).

[42] B. Peng, S. K. Özdemir, S. Rotter, H. Yilmaz, M. Liertzer, F. Monifi, C. M. Bender, F. Nori, and L. Yang Science **346**, 328 (2014).

[43] S. Assawaworrarit, X. Yu, and S. Fan, Nature **546**, 387 (2017).

[44] J. Zhang, B. Peng, S.K. Özdemir, K. Pichler, D.O. Krimer, G. Zhao, F. Nori, Y. Liu, S. Rotter, and L. Yang, Nat. Phot. **12**, 479 (2018).

[45] H. Hodaei, A. U. Hassan, S. Wittek, H. Garcia-Gracia, R. El-Ganainy, D. N. Christodoulides, and M. Khajavikhan, Nature **548**, 187 (2017).

[46] S. Xia, D. Kaltsas, D. Song, I. Komis, J. Xu, A. Szameit, H. Buljan, K.G. Makris, and Z. Chen, Science **372** 72 (2021).

[47] V. V. Konotop, J. Yang, and D. A. Zezyulin, Rev. Mod. Phys. **88**, 035002 (2016).

[48] Y. Ashida, Z. Gong, and M. Ueda, Advances in Physics **69**, 249 (2020).

[49] K.G. Makris, A. Brandstotter, P. Ambichl, Z.H. Musslimani, and S. Rotter, Light: Sci. Appl. **6**, e17035 (2017).

[50] K.G. Makris, I. Kresic, A. Brandstotter, and S. Rotter, Optica **7**, 619 (2020).

[51] A. F. Tzortzakakis, K. G. Makris, and E. N. Economou, Phys. Rev. B **101**, 014202 (2020).

[52] Y. Huang and B. I. Shklovskii, Phys. Rev. B, **101**, 014204 (2020).

[53] A.F. Tzortzakakis, K.G. Makris, S. Rotter, and E.N. Economou, Phys. Rev. A **102**, 033504 (2020).

[54] P. O. Sukhachov and A. V. Balatsky, Phys. Rev. Res., **2**, 013325 (2020).

[55] Y. Liu, X. P. Jiang, J. Cao, J. and S. Chen, Phys. Rev. B, **101**, 174205 (2020).

[56] K. Kawabata, K. and S. Ryu, Phys. Rev. Lett. **126**, 166801 (2021).

[57] H. Liu, Z. Su, Z. Q. Zhang and H. Jiang, Chin. Phys. B (2020).

[58] S. Weidemann, M. Kremer, S. Longhi and A. Szameit, Nat. Phot. **15**, 576 (2021).

[59] A.F. Tzortzakakis, K.G. Makris, A. Szameit, and E.N. Economou, Phys. Rev. Res. **3**, 013208 (2021).

[60] J. Feinberg and A. Zee, Phys. Rev. E **59**, 6433 (1999).

[61] N. Hatano and D. R. Nelson, Phys. Rev. B **56**, 8651 (1997).

[62] N. Hatano and D. R. Nelson, Phys. Rev. B **58**, 8384 (1998).

[63] A. Amir, N. Hatano, and D. R. Nelson, Phys. Rev. E **93**, 042310 (2016).

[64] S. Longhi, D. Gatti, and G. D. Valle, Sci Rep 5, (2015)

[65] Z. Gong, Y. Ashida, K. Kawabata, K. Takasan, S. Higashikawa, and M. Ueda, Phys. Rev. X **8**, 031079 (2018).

[66] L. G. Molinari and G. Lacagnina, J. Phys. A: Math. Theor. **42** 395204 (2009).

[67] L. Li, C. H. Lee, S. Mu, and J. Gong, Nat. Commun. **11**, (2020).

[68] S. Longhi, Phys. Rev. B **103**, 144202 (2021).

[69] K. Zhang, Z. Yang, and C. Fang, Nat. Commun. **13**, (2022).

[70] E. Edvardsson and E. Ardonne, Phys. Rev. B **106**, (2022).

[71] X. Zhang, Y. Tian, J.-H. Jiang, M.-H. Lu, and Y.-F. Chen, Nat Commun **12**, (2021).

[72] L. Martin, G. Di Giuseppe, A. Perez-Leija, R. Keil, F. Dreisow, M. Heinrich, S. Nolte, A. Szameit, A. F. Abouraddy, D. N. Christodoulides, and B. E. A. Saleh, Opt. Express **19**, 13636 (2011).

[73] L. G. Molinari, J. Phys. A Math. Theor. **42**, 265204 (2009).

[74] E. N. Economou and P. D. Antoniou, Solid State Communications **21**, 285 (1977).